THE ASTROPHYSICAL JOURNAL, 556:562–581, 2001 August 1

INTERPRETING THE COSMIC INFRARED BACKGROUND: CONSTRAINTS ON THE EVOLUTION OF THE DUST-ENSHROUDED STAR FORMATION RATE

R. CHARY[1] AND D. ELBAZ[1,2,3]

Received 2001 January 21; accepted 2001 April 5

ABSTRACT

The mid-infrared local luminosity function is evolved with redshift to fit the spectrum of the cosmic infrared background (CIRB) at $\lambda > 5$ μm and the galaxy counts from various surveys at mid-infrared, far-infrared, and submillimeter wavelengths. A variety of evolutionary models provide satisfactory fits to the CIRB and the number counts. The degeneracy in the range of models cannot be broken by current observations. However, the different evolutionary models yield approximately the same comoving number density of infrared luminous galaxies as a function of redshift. Since the spectrum of the cosmic background at $\lambda > 200$ μm is quite sensitive to the evolution at high redshift, i.e., $z > 1$, all models that fit the counts require a flattening at $z \sim 0.8$ to avoid overproducing the CIRB. About 80% of the 140 μm CIRB is produced at $0 < z < 1.5$, while only about 30% of the 850 μm background is produced within the same redshift range. The nature of the evolution is then translated into a measure of the dust-enshrouded star formation rate (SFR) density as a function of redshift and compared with estimates from rest-frame optical/ultraviolet surveys. The dust-enshrouded SFR density appears to peak at $z = 0.8 \pm 0.1$, much sooner than previously thought, with a value of $0.25^{+0.12}_{-0.1}$ $M_\odot$ yr^{-1} Mpc^{-3}, and remains almost constant up to $z \sim 2$. At least 70% of this star formation takes place in infrared luminous galaxies with $L_{IR} > 10^{11}$ $L_\odot$. The long-wavelength observations that constrain our evolutionary models do not strongly trace the evolution at $z > 2$ and a drop-off in the dust-enshrouded SFR density is consistent with both the CIRB spectrum and the number counts. However, a comparison with the infrared luminosity function derived from extinction-corrected rest-frame optical/ultraviolet observations of the Lyman break galaxy population at $z \sim 3$ suggests that the almost flat comoving SFR density seen between redshifts of 0.8 and 2 extends up to a redshift of $z \sim 4$.

Subject headings: diffuse radiation — galaxies: evolution — infrared: galaxies

On-line material: color figures

1. INTRODUCTION

The extragalactic background light (EBL) in the infrared, also referred to as the cosmic infrared background (CIRB), is a record of the emission, absorption, and reradiation of photons integrated over the cosmic history. It provides a valuable constraint on theories of galaxy formation and evolution. The EBL at near-infrared wavelengths is due to redshifted radiation from stars. At mid-infrared (MIR) wavelengths, the background is due to redshifted emission from dust that consists of the polycyclic aromatic hydrocarbon (PAH) features and very small grains (VSGs) transiently heated to $T \sim 200$ K in individual galaxies. At far-infrared (FIR) wavelengths, the dominant contributor is thought to be cold dust ($T \sim 20$ K) that is heated by the ambient interstellar radiation field in galaxies. The recent detection of this background at 2.2, 3.5, 140, and 240 μm using *COBE* DIRBE data and in the 125–2000 μm range using *COBE* FIRAS measurements by various groups (Puget et al. 1996; Dwek & Arendt 1998; Fixsen et al. 1998; Hauser et al. 1998; Schlegel, Finkbeiner, & Davis 1998; Lagache et al. 1999; Gorjian, Wright, & Chary 2000; Wright & Reese 2000; Wright 2001) has indicated that the intensity of the optical/near-infrared background is roughly equal to that of the far-infrared background. This implies that about 50% of the integrated rest-frame optical/UV emission from stars and other objects is thermally reprocessed by dust and radiated at mid- and far-infrared wavelengths. Thus, star formation rates (SFRs) that are derived from rest-frame optical/UV luminosities of galaxies are a lower limit to the true SFR (see, e.g., Madau, Pozzetti, & Dickinson 1998; Meurer, Heckman, & Calzetti 1999; Steidel et al. 1999; Yan et al. 1999).

The first good evidence of this came from the *IRAS* sky survey, which revealed a new population of galaxies with $L_{IR} = L(8\text{–}1000\ \mu\text{m}) \geq 10^{11}$ $L_\odot$ (see review by Sanders & Mirabel 1996). Those with $L_{IR} \geq 10^{12}$ $L_\odot$ were classified as ultraluminous infrared galaxies (ULIGs), while galaxies with 10^{12} $L_\odot > L_{IR} \geq 10^{11}$ $L_\odot$ were classified as luminous infrared galaxies (LIGs).[4] These objects exhibited the largest known SFRs of all local galaxies, but had $\sim$90% of the bolometric luminosity being emitted in the far-infrared (40–500 μm), indicating that dust reprocessing is a significant parameter that needs to be considered in estimates of star formation in certain galaxies (see, e.g., Soifer et al. 1986). However, in the local universe, the integrated bolometric luminosity density of "normal" optically selected galaxies is $L_{Bol} = 4 \times 10^8$ $L_\odot$ Mpc^{-3}, while that of infrared luminous galaxies is $\sim 8 \times 10^6$ $L_\odot$ Mpc^{-3}, i.e., 50 times less (Soifer et al. 1987). This seems to indicate that the contribu-

[1] Department of Astronomy and Astrophysics, University of California at Santa Cruz, 477 Clark Kerr Hall, Santa Cruz, CA 95064; rchary@ucolick.org, elbaz@ucolick.org.

[2] CEA Saclay, DAPNIA, Service d'Astrophysique, Orme des Merisiers, 91191 Gif-sur-Yvette, Cédex, France.

[3] Physics Department, University of California at Santa Cruz, Santa Cruz, CA 95064.

[4] Previously, the term LIG was used for all objects with $L_{IR} \geq 10^{11}$ $L_\odot$. We use "infrared luminous galaxies" when referring to both LIGs and ULIGs collectively.

tion from LIGs and ULIGs is sufficiently small that they need to be considered only as extreme cases.

Spectroscopic follow-up of the faint *IRAS* population that covered a relatively small redshift range ($z < 0.27$) indicated that infrared luminous galaxies were more numerous in the past than they are today and may make a significantly larger contribution to the integrated luminosity density than inferred from observations of the local universe (Kim & Sanders 1998). Deeper observations that trace the far-infrared luminosity of galaxies to high redshift are difficult since cirrus and confusion noise rapidly begin to dominate.

The ISOCAM guaranteed-time extragalactic surveys in conjunction with the European Large Area *ISO* Survey (ELAIS) and observations of the lensing cluster Abell 2390 covered a range of flux densities between 50 μJy and 50 mJy at 15 μm (Altieri et al. 1999; Elbaz et al. 1999; Serjeant et al. 2000). The differential counts resulting from these surveys revealed that the counts of galaxies increase quite rapidly as S_ν^{-3} at brighter flux levels ($S_\nu > 0.4$ mJy) and then flatten out as $S_\nu^{-1.6}$ at fainter levels. The observed mid-infrared counts are an order of magnitude higher than expected if the local mid-infrared luminosity function was not evolving with redshift. This rapid increase in mid-infrared luminous galaxies has been modeled as a $(1 + z)^{4.5}$ luminosity evolution in the 15 μm local luminosity function (LLF) by Xu (2000) and as a combination of number density and luminosity evolution by Franceschini et al. (2001). This evolution is much stronger than observed in the UV by Cowie, Songaila, & Barger (1999), who find that the comoving UV luminosity density evolves as $(1 + z)^{1.5}$ instead of the $(1 + z)^{3.9 \pm 0.75}$ initially proposed by Lilly et al. (1996). Furthermore, observations of galaxies in the local universe have shown that the mid-infrared and infrared luminosities are well correlated (§ 2). The mid-infrared luminosity of $\sim$70% of the sources seen in the ISOCAM surveys, particularly in the Hubble Deep Field–North and flanking fields (HDF-N + FF), translates to an infrared luminosity greater than $10^{11}\ L_\odot$, implying that the majority of them are LIGs and ULIGs (Elbaz et al. 2001). At $z \sim 0.8$, the mid-infrared luminosity density derived from the ISOCAM 15 μm sources is $\sim 7 \times 10^7\ L_\odot\ \mathrm{Mpc}^{-3}$, while the 8–1000 μm luminosity density adopting the mid- to far-infrared correlation seen in the local universe is $\sim 5 \times 10^8\ L_\odot\ \mathrm{Mpc}^{-3}$. In comparison, at $z \sim 0$, LIGs and ULIGs contribute $10^6\ L_\odot\ \mathrm{Mpc}^{-3}$ to the 12 and 15 μm luminosity density and $7.8 \times 10^6\ L_\odot\ \mathrm{Mpc}^{-3}$ to the infrared luminosity density, as derived from the LLF of Soifer et al. (1987), Fang et al. (1998), and Xu et al. (1998). This indicates an increase by a factor of about 60 between $z \sim 0$ and $z \sim 0.8$, providing further evidence for an evolution in the infrared luminosity function (IRLF) with redshift.

Similar deep surveys have been conducted at 850 μm using the Submillimeter Common-User Bolometer Array (SCUBA) instrument on the James Clerk Maxwell Telescope (Hughes et al. 1998; Barger, Cowie, & Sanders 1999; Blain et al. 1999a; Eales et al. 2000). The large beam size (14″ FWHM) and the negative k-correction in this wavelength regime make identification of the optical counterparts and thereby the redshift distribution of the sources very difficult. High-resolution radio interferometric observations and the use of 450 μm/850 μm flux ratios have helped somewhat to localize the sources and constrain the redshifts (Hughes et al. 1998; Barger, Cowie, & Richards 2000). These have placed the bright ($S_\nu > 6$ mJy) submillimeter sources at $z \sim 1$–3, which has been confirmed by the more extensive survey of Chapman et al. (2001). The implication of this is that most, if not all, of the submillimeter sources are extreme ULIGs with SFRs of 10^2–$10^3\ M_\odot\ \mathrm{yr}^{-1}$. Furthermore, the SFR density due to ULIGs must have increased by about 2 orders of magnitude between $z \sim 0$ and $z \sim 1$–3.

Many of the LIGs and ULIGs in the local universe show morphological signatures of interaction, and more than 50% of the optical counterparts of ISOCAM HDF-N galaxies show evidence for interactions (Mann et al. 1997). Surveys at visible wavelengths show a redshift evolution of the merger fraction, defined as the fraction of close pairs of galaxies, as $\sim(1 + z)^3$ (see, e.g., Le Fèvre et al. 2000). Thus, if mergers were indeed a tracer of LIGs and ULIGs, this would again suggest that the bright end of the IRLF is evolving strongly. However, the faint end of the IRLF is very poorly constrained at $z \sim 1$ since none of the long-wavelength surveys are sensitive enough to detect galaxies with $L_{\mathrm{IR}} < 10^{11}\ L_\odot$ at $z > 0.5$. Meurer et al. (1999) have shown that the FIR-to-UV flux ratio is closely related to the UV slope for normal starbursts but that the relationship breaks down for ULIGs (Meurer et al. 2001). This indicates that the visible/near-infrared counts can potentially place constraints on the evolution of the faint end of the IRLF, but we postpone this discussion to the future.

In this paper, we combine data from a variety of published surveys of nearby galaxies to determine the correlation, if any, between the luminosities at various mid- and far-infrared wavelengths. We use these correlations to generate smoothly varying spectral energy distributions (SEDs) for galaxies as a function of luminosity class. We assess the need for luminosity and density evolution in the 15 μm luminosity function of Xu et al. (1998) and therefore the 60 μm luminosity function of Soifer et al. (1987) based on fits to the ISOCAM 15 μm, ISOPHOT 90 and 170 μm, and SCUBA 850 μm galaxy counts as well as the spectrum of the CIRB at $\lambda > 5$ μm. The evolution of the mid-IR LF is then translated to an estimate of the dust-enshrouded SFR density as a function of redshift and compared with SFR values derived from optical/near-infrared surveys. We adopt an $H_0 = 75\ \mathrm{km\ s}^{-1}\ \mathrm{Mpc}^{-1}$, $\Omega_M = 0.3$, $\Omega_\Lambda = 0.7$ cosmology throughout this paper unless otherwise explicitly stated.

2. LUMINOSITY CORRELATIONS IN THE INFRARED AND TEMPLATE SPECTRAL ENERGY DISTRIBUTIONS

It can be shown that the 12 μm and far-infrared luminosities of galaxies in the *IRAS* Bright Galaxy Sample (BGS) cannot be accurately derived from their B-band luminosities (Soifer et al. 1987).[5] The peak-to-peak scatter in the L_B/L_{IR} ratio for a fixed L_{IR} is about a factor of 20. However, as mentioned earlier, the FIR-to-UV flux ratio has been shown to be closely related to the UV slope for normal starbursts (Meurer et al. 1999). This relationship breaks down for the ULIGs (Meurer et al. 2001). The phenomenon can be qualitatively explained by the fact that the UV emission arises from stars that are relatively unobscured to the observer. Regions of star formation with a large optical

[5] The Zwicky magnitudes m_Z in the BGS were converted to B luminosities using $m_B = m_Z - 0.14$ and a B-band zero point of 4260 Jy.

depth, i.e., H II regions, could exist in the central regions of galaxies where almost all the UV light is reprocessed to the MIR and FIR. Thus, the regions of FIR and UV emission would be unrelated, especially for ULIGs. The best observational evidence for this explanation can be seen in the Antennae galaxy (Mirabel et al. 1998), in which about half the 15 μm emission seen by ISOCAM arises from regions that are inconspicuous at visible wavelengths. The breakdown in the FIR-to-UV slope correlation for ULIGs is problematic for the determination of the true SFR from optical/UV surveys since submillimeter observations using the SCUBA instrument indicate that ULIGs might have a larger contribution to the SFR density at high redshift. This suggests that it will be difficult to determine the true SFR by applying an accurate extinction correction to the optical/UV-determined value.

Since the short-wavelength starlight and dust emission are not closely related, an estimate of the dust-enshrouded SFR can only be derived from other tracers, such as the mid-infrared and far-infrared luminosities, or by using the radio–to–far-infrared correlation shown by Condon (1992). In the mid-infrared regime, the spectra of galaxies exhibit broad emission features at 6.2, 7.7, 8.6, 11.3, and 12.7 μm, which are probably from PAHs (see review by Puget & Leger 1989). These features and their associated continuum dominate the emission at mid-infrared wavelengths shortward of 10 μm. There is, in addition, a continuum from VSGs of size less than 10 nm, that dominates the emission above ~ 10 μm (Désert, Boulanger, & Puget 1990; Laurent et al. 2000) except for quiescent star-forming galaxies. The VSGs get transiently heated to temperatures of ~ 200 K by the ambient optical/UV continuum, which is proportional to the star formation activity. In addition, mid-infrared measurements do not need large extinction corrections since the extinction at mid-infrared wavelengths is only about 1% of that at visible wavelengths (Mathis 1990). The radio wavelengths, on the other hand, are dominated by free-free emission from H II regions and synchrotron emission from supernova remnants. Although radio observations are almost confusion-limited at an 8.5 GHz sensitivity of 9 μJy obtained over the HDF (Richards et al. 1998), we find that they are typically as sensitive as the ISOCAM 15 μm observations in that they can typically probe galaxies with $L_{\rm IR} \sim 10^{11.4}\ L_\odot$ at $z \sim 1$. Since the ISOCAM 15 μm observations provide the primary constraint on evolution models at $z < 1.2$, we adopt as a starting point the local 15 μm luminosity function described in Xu et al. (1998) and Xu (2000). For the rest of this paper, we will use the convention defined in Sanders & Mirabel (1996):

$$L_{\rm IR} = L(8\text{–}1000\ \mu\text{m}) = 1.8 \times 10^{-14} \times 10^{26} (13.48L_{12} + 5.16L_{25} + 2.58L_{60} + L_{100}) \quad (1)$$

$$L_{\rm FIR} = L(40\text{–}500\ \mu\text{m}) = 1.6 \times 1.26 \times 10^{-14} \times 10^{26}\ (2.58L_{60} + L_{100})\,. \quad (2)$$

In the above equations, the symbol L_λ is defined as $L_\nu(\lambda\ \mu\text{m})$ in units of $L_\odot\ \text{Hz}^{-1}$. $L_{\rm IR}$ and $L_{\rm FIR}$ are in $L_\odot$.

To use the mid-IR LF as a tracer of the dust-enshrouded SFR, we first need to define a calibration scale. Figures 1 and 2 illustrate the accuracy with which the infrared luminosity of galaxies can be derived from their mid-infrared luminosities. Figure 1 is based on ~ 300 galaxies from the *IRAS* BGS, while Figure 2 is based on published ISOCAM and ISOPHOT observations of *IRAS* galaxies. The data points with $L_{\rm IR} > 10^{10}\ L_\odot$ are fitted by a first-order polynomial shown in equations (4)–(6). This is shown as a solid black line in the upper panels of the figure. Objects with $L_{\rm IR} < 10^{10}\ L_\odot$ are not used for the fits. At these low luminosities, the fraction of the bolometric luminosity emitted in the infrared is less than 50%; i.e., visible starlight that is not obscured by dust is dominating the radiated energy of the galaxy. On the other hand, a significant fraction of the more luminous objects shows disturbed morphologies, suggesting interactions with other galaxies that would result in gas-rich systems with star formation in highly obscured regions. The lower plots in both figures show the scatter in the ratio of the infrared luminosity as derived from *IRAS* data for these galaxies to the infrared luminosity derived from the polynomial fits. Also shown is the 1 σ uncertainty in the derived infrared luminosity calculated as the range within which 68% of the galaxies lie. The lowest luminosity objects ($L_{\rm IR} < 10^9\ L_\odot$) have been rejected in the lower plots.

The 6.7 μm luminosities were derived from *Infrared Space Observatory* (*ISO*) observations of ~ 90 nearby starburst-dominated galaxies. Forty-four spiral and starburst galaxies had photometry from ISOCAM (P. Chanial et al. 2001, in preparation; Roussel et al. 2001; Laurent et al. 2000), eight ULIGs had spectra from ISOCAM circular variable filter (CVF) observations (Tran et al. 2001), while 37 ULIGs had ISOPHOT mid-infrared spectra (Rigopoulou et al. 1999). Rigopoulou et al. (1999) obtained mid-infrared spectra with ISOPHOT of about 60 ULIGs and about 15 low-luminosity starbursts and normal galaxies to study the emission features from the PAHs. Of the 60 ULIGs, about 45 had the 7.7 μm PAH feature detected with a good signal-to-noise ratio. However, the calibration and performance of the instrument is not very well determined. To assess the quality of the data set, we compared the ISOPHOT observations on five ULIGs and four low-luminosity starbursts/normal galaxies to the P. Chanial et al. (2001, in preparation) ISOCAM LW2 observations of the same galaxies.[6] We find that for the ULIGs, the ratio of 7.7 μm line + continuum flux density as published in Rigopoulou et al. to the ISOCAM 6.7 μm flux density lies in the 1.5–3.0 range. In comparison, for the starbursts/normal galaxies, the ratio of 7.7 μm line + continuum to the ISOCAM 6.7 μm flux density falls in the 0.2–1.6 range, a factor of 8. So, for assessing the correlation between the mid- and far-infrared luminosities, we consider the ISOCAM data on bright *IRAS* galaxies as well as the ULIG sample of Rigopoulou et al. (1999), dividing the line + continuum flux value published in the latter by 2.4 and assigning a peak-to-peak error bar of a factor of 2. This is consistent with the range of 1.5–2.7 that we find for the 7.7 μm line + continuum to the 6.7 μm flux density ratio in the ISOCAM CVF observations of Tran et al. (2001).

The 15 μm and infrared luminosities of 120 *IRAS* galaxies were taken from the sample of P. Chanial et al. (2001, in preparation) and the survey performed in the north ecliptic pole region (NEPR) by Aussel et al. (2000). The NEPR sample of galaxies only has *IRAS* 60 μm luminosities available, and we have converted these to a far-infrared lumi-

[6] The LW2 filter is broad enough to include the 7.7 μm PAH feature but is centered at 6.75 μm.

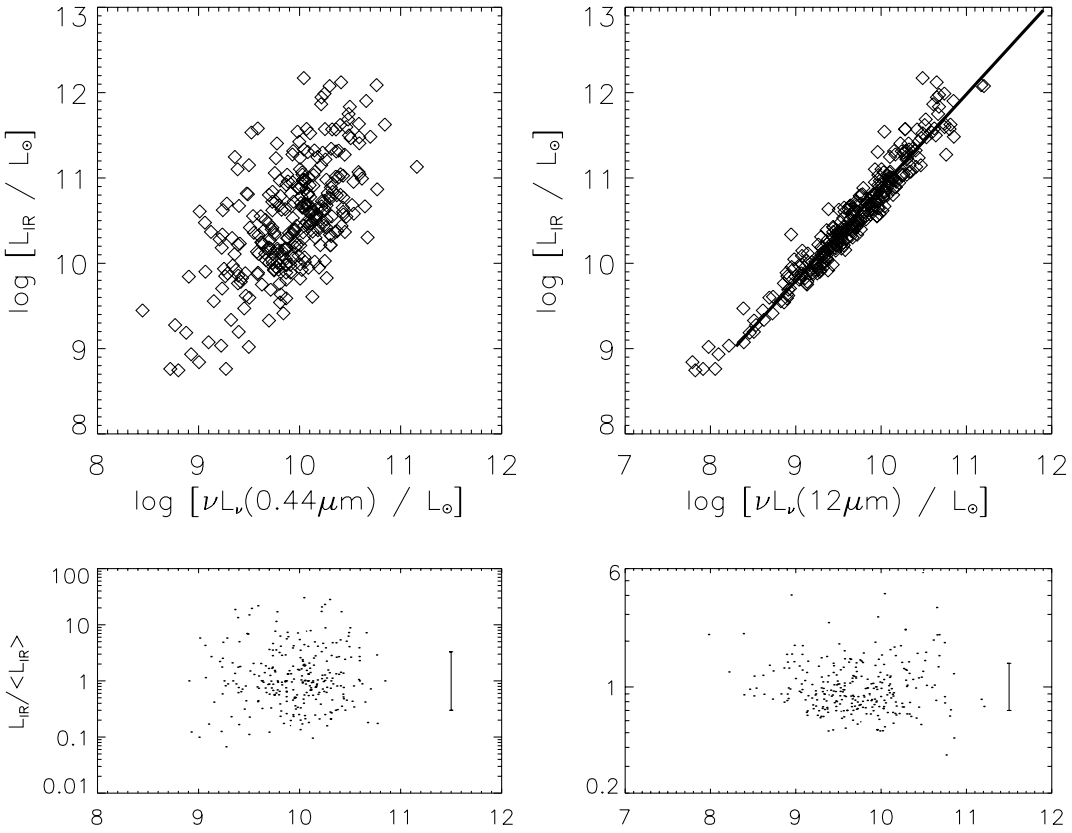

FIG. 1.—Plots showing the relative accuracy of tracing infrared luminosities (8–1000 μm) of *IRAS* BGS (Soifer et al. 1987) objects from the *B*-band (0.44 μm) and 12 μm luminosities. The lower plots show the ratio between the true infrared luminosity (L_{IR}) and the predicted infrared luminosity ($\langle L_{IR} \rangle$) derived from the *B*-band or 12 μm luminosity using a first-order polynomial fitted to data points with $L_{IR} > 10^{10}\ L_{\odot}$. If the infrared luminosity of all galaxies could be predicted precisely from their *B*-band or 12 μm luminosity, then all points in the lower plot would lie in a horizontal line with $L_{IR}/\langle L_{IR} \rangle = 1$. The lower plots also show the 1 σ uncertainty in the prediction of the infrared luminosities.

nosity based on a 60 μm–to–far-infrared correlation derived by combining the *IRAS* BGS and the *IRAS* Point-Source Catalog Redshift survey (PSCz) of Saunders et al. (2000). The far-infrared luminosity is typically about 83% of the total infrared luminosity, and we have applied this conversion to be consistent with the other plots.

Clearly, the 6.7, 12, and 15 μm luminosities of galaxies trace the infrared luminosity much better than the *B*-band luminosity. The 15 μm–to–IR and 12 μm–to–IR correlations were determined from a first-order polynomial fitted to the data with $L_{IR} > 10^{10}\ L_{\odot}$. Since the 6.7 μm–to–IR correlation is based on different data sets from CVF and broadband photometry with ISOCAM and spectroscopy using ISOPHOT, the polynomial fit for the 6.7 μm–to–IR correlation was determined by applying a *k*-correction from 6.7 to 15 μm based on ISOCAM observations of nearby galaxies (Fig. 3) and then using the 15 μm–to–IR correlation. The mid-infrared–to–IR correlations show a similar scatter around the correlation line, which is about a factor of 5 better than the optical-to-IR correlation.

These data sets tentatively illustrate the potential of using the mid-infrared as a tracer of dust-enshrouded star formation, and a more homogeneous and comprehensive survey of nearby galaxies, as will be undertaken by the *Space Infrared Telescope Facility* (*SIRTF*), will be required to either strengthen or reject this correlation.

Kennicutt (1998) has transformed the infrared luminosity of young (age $< 10^8$ yr) starburst galaxies to an SFR. If we adopt the correlations shown in the previous figures, we can translate the mid-infrared luminosity of galaxies with $L_{IR} > 10^{10}\ L_{\odot}$ to an approximate estimate of the dust-enshrouded SFR (ρ') using the formula

$$\rho'(M_{\odot}\ \mathrm{yr}^{-1}) = 1.71 \times 10^{-10} L_{IR}\ (L_{\odot})\,, \quad (3)$$

$$L_{IR} = 11.1^{+5.5}_{-3.7} L_{15\,\mu m}^{0.998}\,, \quad (4)$$

$$L_{IR} = 0.89^{+0.38}_{-0.27} L_{12\,\mu m}^{1.094}\,, \quad (5)$$

$$L_{IR} = 4.37^{+2.35}_{-2.13} 10^{-6} \times L_{6.7\,\mu m}^{1.62}\,, \quad (6)$$

where all values are in units of solar luminosity. The 1 σ values have been estimated by calculating the range of values within which 68% of galaxies have their observed infrared luminosities.

As mentioned earlier, the main observational constraints on models that trace the redshift evolution of the IRLF are the following:

1. Differential counts from various surveys at mid-infrared, far-infrared, and submillimeter wavelengths.
2. The spectrum of the CIRB at $\lambda > 5$ μm.

To use these constraints, it is necessary to know the luminosity at different wavelengths for galaxies in each luminosity bin of the IRLF. This motivates the generation of template spectra for objects of different luminosity classes. It is useful to note that many evolutionary models that have already been developed either use a mid-infrared template

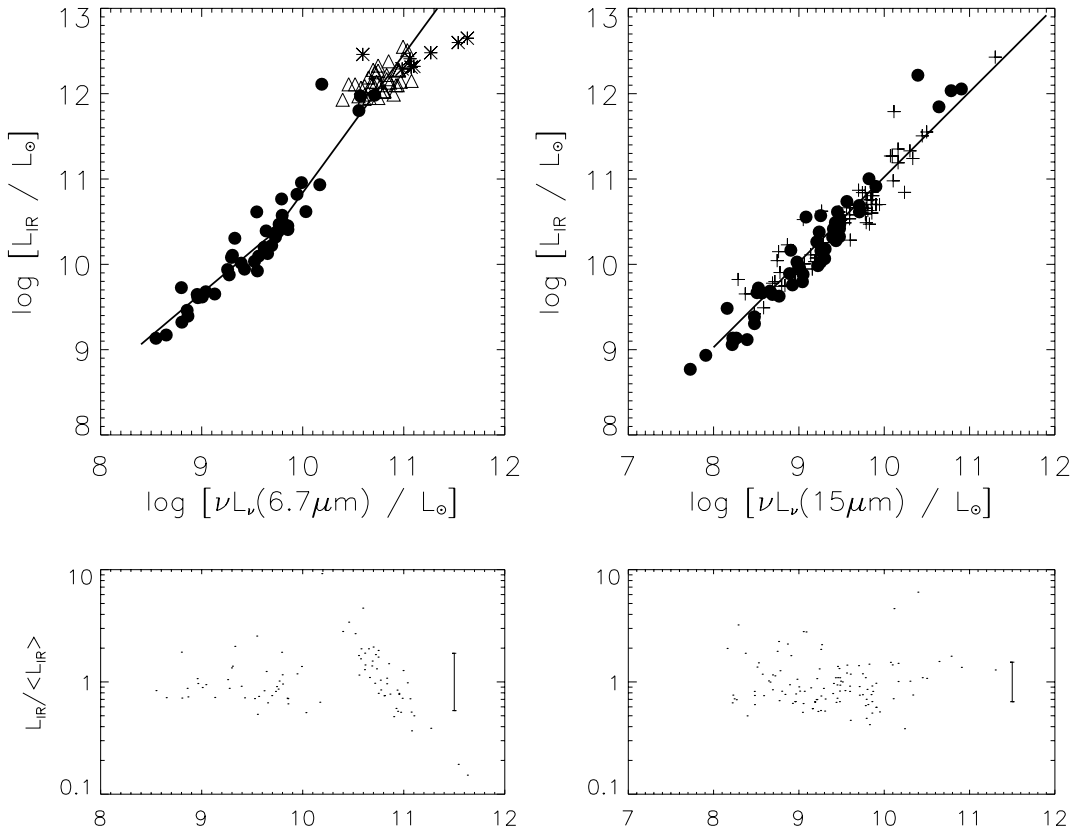

FIG. 2.—Plots showing the relative accuracy of tracing infrared luminosities (8–1000 μm) from the 6.7 and 15 μm luminosities. The 6.7 μm luminosities are from ISOCAM guaranteed-time surveys (*filled circles*; P. Chanial et al. 2001, in preparation) and ISOPHOT 7 μm spectroscopy of ULIGs (*open triangles*) by Rigopoulou et al. (1999). Note that the Rigopoulou et al. (1999) values have been modified as described in the text. Asterisks are the 6.7 μm luminosities for the starburst-dominated ULIG sample of Tran et al. (2001). Some of the extreme ULIGs might have a significant AGN contribution, which could result in a deviation from the 6.7 μm–to–IR correlation derived for starbursts by decreasing the IR luminosity for a given 6.7 luminosity, as for the two brightest galaxies in our sample. The 15 μm luminosities are from the P. Chanial et al. (2001, in preparation; *filled circles*) and the Aussel et al. (2000; *plus signs*) sample of galaxies. The lower plots are similar to those in Fig. 1.

that is a very poor representation of the true PAH emission features (e.g., Rowan-Robinson 2001; Pearson 2001; Sadat, Guiderdoni, & Silk 2001) or neglect the PAH features altogether (Malkan & Stecker 1998, 2001). It is trivial to show that this makes a critical difference in the quality of the fits to the ISOCAM mid-infrared number counts and therefore affects the evolution parameters, particularly at $z < 1$. So, it is important to have template SEDs that reproduce the observed trend in the luminosity of local galaxies at different wavelengths.

Using MIR, FIR, and submillimeter data from ISOCAM, *IRAS*, and SCUBA observations of nearby galaxies, we fitted the observed trend between different mid- and far-infrared luminosities, as shown in Figure 3. The top two panels in the figure show the ISOCAM observations at 6.7 and 15 μm for $\sim$50 *IRAS* galaxies that are described in P. Chanial et al. (2001, in preparation). The solid lines in the panels show two first-order polynomial fits, one for galaxies with 15 μm luminosity less than $2 \times 10^9\ L_\odot$ and another for more luminous galaxies. This is because the ratio between the mid-infrared luminosities changes as a function of the 15 μm luminosity, possibly because of enhanced emission from the VSG component (Laurent et al. 2000). The luminosity break corresponds to $L_{\rm IR} \sim 2 \times 10^{10}\ L_\odot$, which is similar to the luminosity cutoff used for deriving equations (4)–(6). The panel showing the 15–60 μm trend consists of data described in Figure 2. The 60 μm–to–FIR correlation is for the *IRAS* BGS and PSCz galaxies, while the panel showing the IR-to-FIR correlation is only for the *IRAS* BGS galaxies. The last panel shows SCUBA submillimeter data on $\sim$100 *IRAS* galaxies (Dunne et al. 2000). In addition, the correlation between *IRAS* 25 and 100 μm luminosities for galaxies in the BGS was also determined. The solid lines for the four lower panels utilize only a single first-order polynomial fitted to all the data points. Also shown in the panels as triangles are the luminosities at the corresponding wavelength for the different templates that were generated as described below.

Template SEDs were generated between 0.1 and 1000 μm to reproduce the observed trend between mid-infrared and far-infrared luminosities. To generate these templates, we used the basic Silva et al. (1998) models to reproduce the ultraviolet-submillimeter SED of four prototypical galaxies—Arp 220, NGC 6090, M82, and M51. These correspond to objects of four different luminosity classes—ULIGs, LIGs, "starbursts" (SBs) and "normal galaxies," respectively. ISOCAM CVF observations between 3 and 18 μm of these galaxies provided new data on the relative strength of the mid-infrared features and continuum (Charmandaris et al. 1999; Laurent et al. 2000; Forster-Schreiber et al. 2001; Roussel et al. 2001). The mid-infrared region of the modeled spectra were then replaced with the ISOCAM observations. In addition, corrections were made for the 17.9 μm silicate feature based on observations by

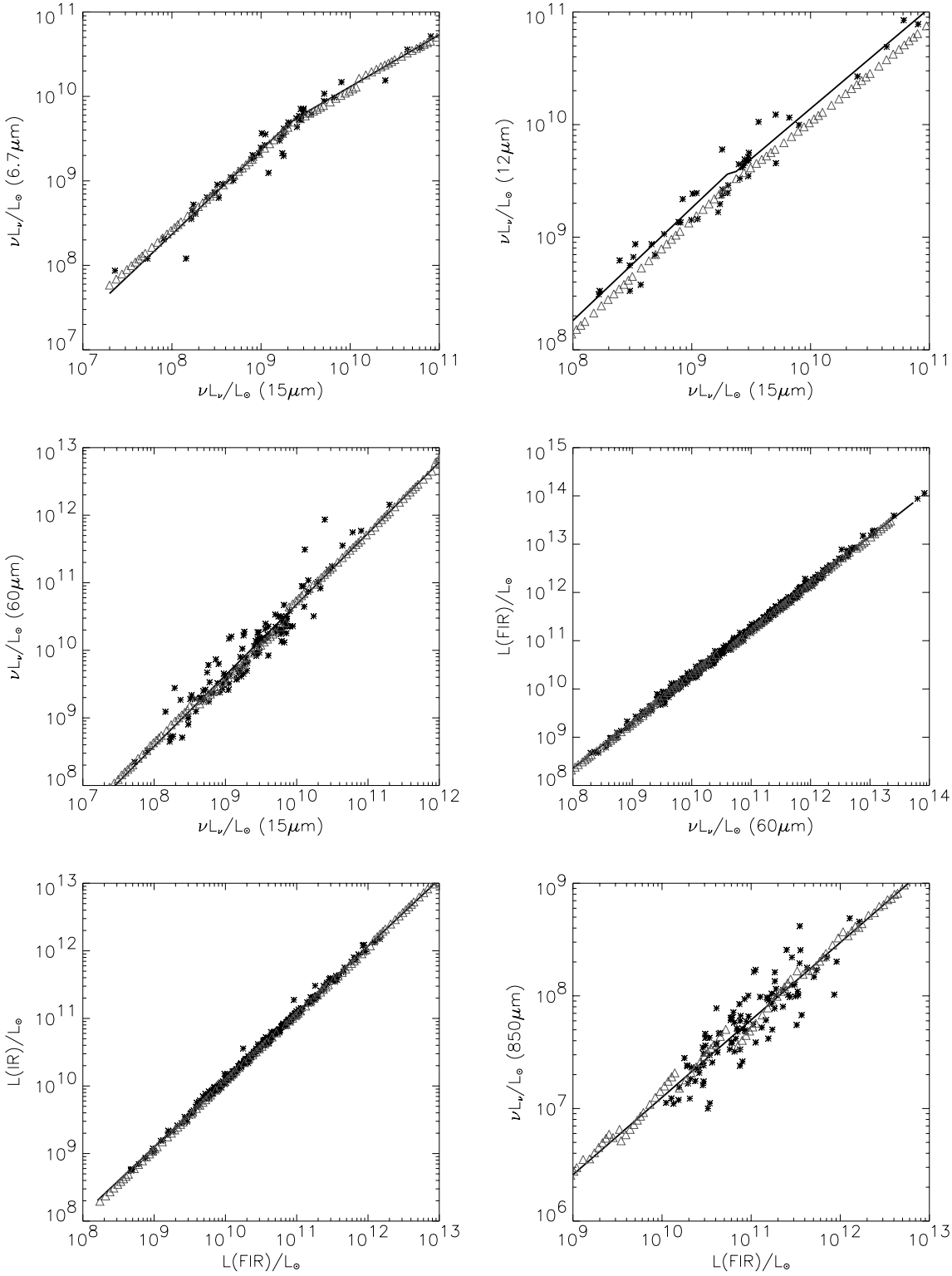

FIG. 3.—Plot showing the data (*asterisks*) at different wavelengths from *IRAS*, ISOCAM, and SCUBA surveys (Soifer et al. 1987; Aussel et al. 2000; Dunne et al. 2000; Saunders et al. 2000; P. Chanial et al. 2001, in preparation). The lines are the best-fit polynomial of order 1. The triangles are the corresponding values from our template SEDs that were generated as described in the text. [*See the electronic edition of the Journal for a color version of this figure.*]

Smith, Aitken, & Roche (1989). The four template spectra were checked to ensure that the *IRAS* observed values of these four galaxies were reproduced. We then partitioned the four templates into a mid-infrared (4–20 μm) and far-infrared (20–1000 μm) component and interpolated between the four to generate a range of mid- and far-infrared sample templates of intermediate luminosity. An additional set of far-infrared templates provided by Dale et al. (2001) were added to the ensemble of far-infrared templates to span a wider range of spectral shapes.

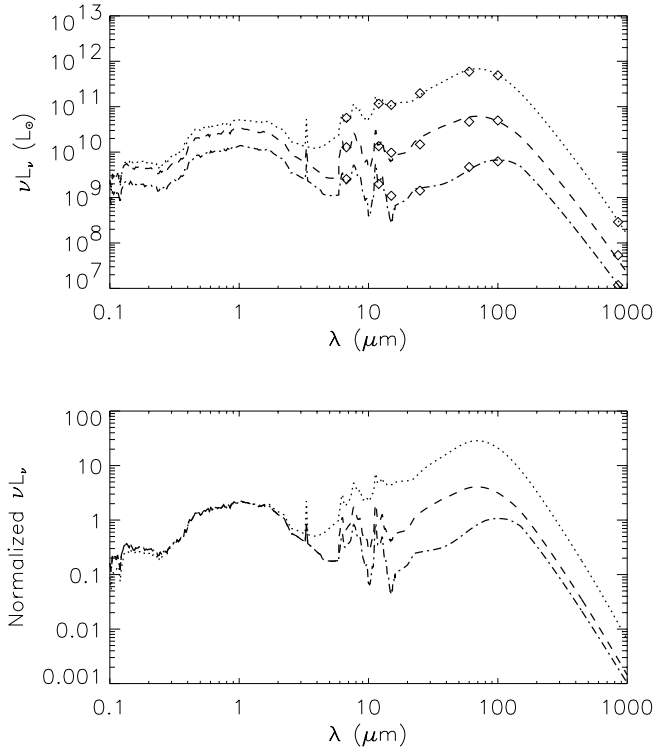

FIG. 4.—Template SED for objects of three different infrared luminosities along with the predicted luminosities at different wavelengths (*diamonds*). The luminosities correspond to $L_{IR} = 10^{12}$, 10^{11}, and $10^{10}\ L_\odot$, illustrating the SED of ULIGs, LIGs, and starbursts, respectively. The lower plot shows the same templates, normalized at 0.44 μm (*B* band) to show the evolution of the spectrum as a function of infrared luminosity. No correction for the UV slope has been made.

For each luminosity bin of the 15 μm luminosity function, the luminosities at the following wavelengths, 6.7, 12, 25, 60, 100, and 850 μm, were predicted based on the polynomial fits to the data shown in Figure 3. Of the ~100 mid-infrared sample templates generated as described above, the mid-infrared template that best fits the predicted 6.7, 12, and 15 μm luminosities was selected. Similarly, the far-infrared template that best fits the predicted 25, 60, 100, and 850 μm luminosities was selected. The luminosity of the templates at the corresponding wavelengths was determined by integrating over the filter curves of the instruments. Our goal was only to generate SEDs that reproduce the observed trend in luminosities at different wavelengths. Selecting a variety of sample templates provided better fits to the predicted luminosities than by just interpolating between the four SEDs generated by the Silva et al. (1998) models. The best-fitting mid-infrared and far-infrared templates were then merged together to provide the final template SED for each luminosity bin. The red triangles in Figure 3 are the luminosities at the corresponding wavelengths from the final merged template SEDs. The *B*-band luminosity of galaxies in the *IRAS* BGS shown in Figure 1 was also used to constrain the optical/near-infrared SED of galaxies, but, as stated before, we have not constrained the UV slope of the template SEDs. The absence of a good correlation between the *B*-band and IR luminosities implies that the optical/near-infrared part of our SEDs is highly uncertain. This is not a major problem since we are only analyzing the dust emission in this paper. The templates for three objects with infrared luminosities of 10^{10}, 10^{11}, and $10^{12}\ L_\odot$ along with the predicted luminosities at different wavelengths based on the correlations in Figure 3 are shown in Figure 4.

3. EVOLUTION OF THE 15 μm AND FAR-INFRARED LOCAL LUMINOSITY FUNCTION

Since our intention is to use the different mid- and far-infrared observational constraints to estimate the evolution of the dust-enshrouded SFR with redshift, we use the 15 μm LLF as a tracer of dust emission in the local universe. Xu et al. (1998) and Xu (2000) derived a 15 μm LLF based on a correlation between ISOCAM mid-infrared and *IRAS* mid- and far-infrared data. In addition, estimates of the 12 μm LLF have been made by Rush, Malkan, & Spinoglio (1993) and Fang et al. (1998). The different 12 and 15 μm luminosity functions are shown in Figure 5. Also shown is the predicted 60 μm LLF derived from the mid-infrared LLF using a mid-infrared–to–60 μm conversion from the polynomial fit to the observations of Aussel et al. (2000) and P. Chanial et al. (2001, in preparation) described earlier. All these are in good agreement with each other since they were essentially derived from *IRAS* observations of nearby galaxies.

Evolution of the luminosity function with respect to redshift can be expressed as

$$\Psi(L, z) = n(z)\phi(L, z)\ , \tag{7}$$

$$\phi(L, z) = \phi\left[\frac{L}{g(z)}, 0\right], \tag{8}$$

where $\Psi(L, z)$ is the number density of galaxies as a function of luminosity L and redshift z. The $n(z)$ term represents evolution in the number density of galaxies, while the $\phi(L, z)$ term represents luminosity evolution. The term $\phi(L, 0)$ is the LLF. We consider models where $n(z)$ is of the form $n(0)$ $(1 + z)^{\alpha_D}$ up to a turnover redshift $z^D_{\rm turn}$ followed by $n(z^D_{\rm turn})$ $[(1 + z)/(1 + z^D_{\rm turn})]^{\beta_D}$ up to $z = 4.5$. The luminosity evolution component $g(z) = (1 + z)^{\alpha_L}$ up to $z^L_{\rm turn}$ followed by $g(z^L_{\rm turn})[(1 + z)/(1 + z^L_{\rm turn})]^{\beta_L}$.

It should be emphasized that there is considerable degeneracy in the density and luminosity evolution of galaxies. While density evolution slides the luminosity function along the vertical axis, the latter slides it along the horizontal axis. However, current observations at mid- and far-infrared wavelengths detect galaxies only at the luminous end of the luminosity function, as a result of which, the two are indistinguishable. This is shown in Figure 6. The figure also shows that evolving just the luminous end of the LLF, i.e., $L > 5 \times 10^{10}\ L_\odot$, which is similar to the model proposed by Dole et al. (2000), would result in the same degeneracy with observations, although it would result in a somewhat unphysical break in the luminosity function.

There is an additional degeneracy induced by the fraction of the luminosity function that is evolving. Redshift measurements of ISOCAM 15 μm sources in the HDF-N + FF indicate that the majority of them are LIGs and ULIGs (Elbaz et al. 2001). Interestingly, when the local 60 μm luminosity function is compared to the Schechter function commonly used to represent the LLF at visible wavelengths, an excess of galaxies is seen in the 60 μm LLF beyond $L_{60\,\mu m} > 10^{11}\ L_\odot$ since the Schechter function drops faster at the bright end. On one hand, it seems likely that just this excess of galaxies, most of which show morphological signatures of merger activity, could be evolving at high redshift.

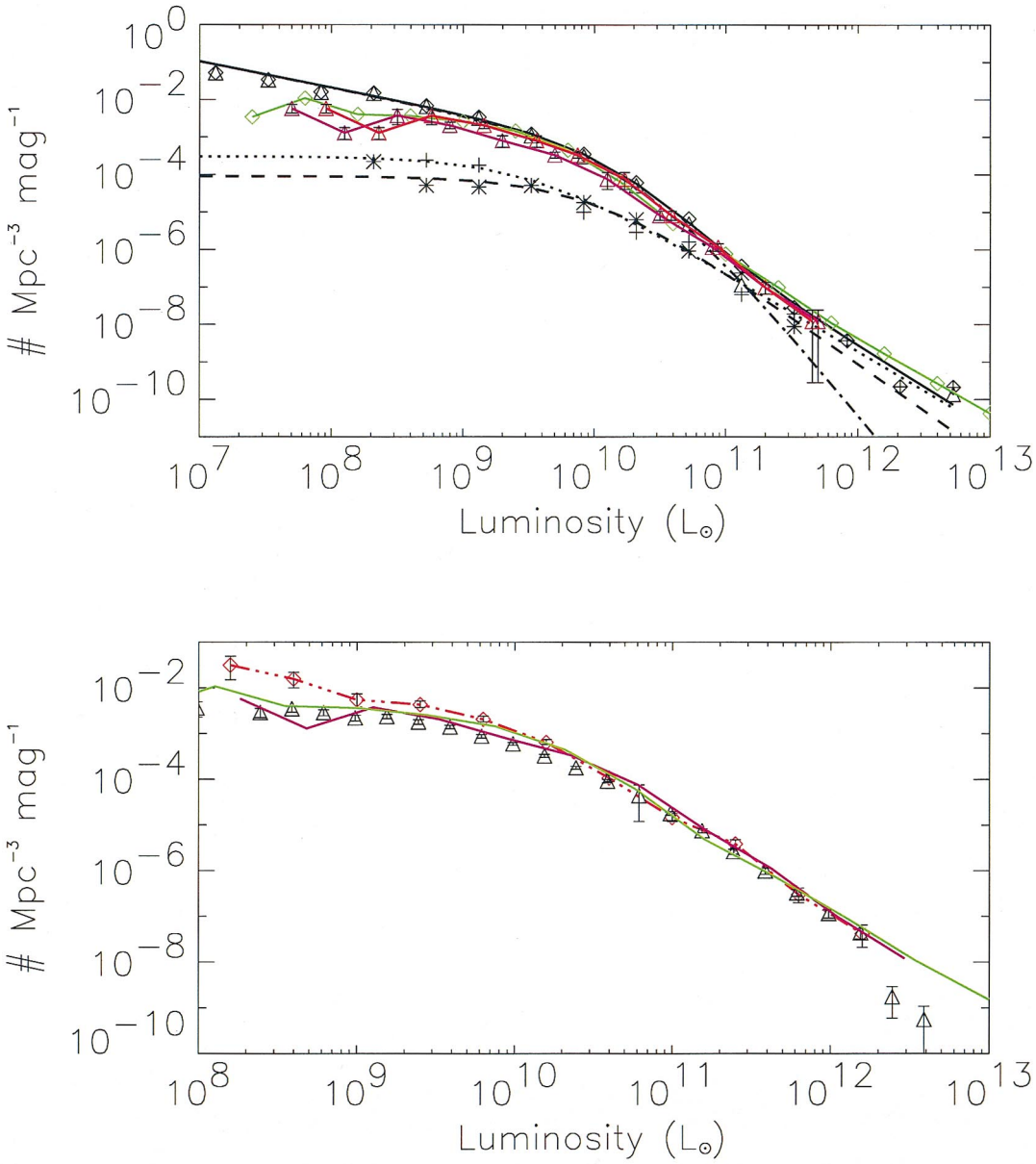

FIG. 5.—Various 12 and 60 μm LLFs for $H_0 = 75$ km s^{-1} Mpc^{-1}. In the upper plot, the black lines and symbols represent the 12 μm LLF from Rush et al. (1993). The solid black line is the total LLF, the black dot-dashed line is the non-Seyfert contribution, the dotted line is from Seyfert 1 galaxies, and the dashed line is from Seyfert 2 galaxies. The green line and symbols are the 12 μm LLF from Fang et al. (1998). The purple line and triangles are the 15 μm LLF from Xu et al. (1998) and Xu (2000). The red line is this 15 μm LLF converted to 12 μm based on a k-correction derived from ISOCAM observations of 44 nearby galaxies. The lower plot shows the 60 μm LLF from Soifer et al. (1987) as the dashed red line, the 60 μm LLF of Saunders et al. (1990) as the black triangles, the 12 μm LLF of Fang et al. (1998) converted to 60 μm using a linear 12 μm–to–60 μm correlation based on *IRAS* BGS data as the green line, and the Xu et al. (1998) 15 μm LLF converted to 60 μm as the purple line.

Alternatively, it is possible that a luminosity-dependent fraction that approaches 100% at $L_{60\,\mu\mathrm{m}} > 10^{11}\ L_\odot$ of the LLF could be evolving. Unfortunately, the observational constraints on the faint end of the IRLF are limited since these galaxies are undetected at mid- and far-infrared wavelengths at $z > 0.5$. The correlation between mid-infrared and visible wavelengths being poor, the counts of galaxies at visible/near-infrared wavelengths cannot be used to constrain the distribution. However, we will investigate in a future paper if the relationship between the FIR/UV flux ratio and UV slope can constrain the evolution of the faint end of the IRLF.

The principal observational constraints on the evolution of the bright end of the luminosity function then are the following:

1. The ISOCAM differential number counts at 15 μm, especially the "knee" in the counts slope at 0.4 mJy (Elbaz et al. 1999).
2. The 15 μm EBL, which has a lower limit from *ISO* counts and an upper limit from gamma-ray observations of a TeV flare in Markarian 501.
3. The redshift distribution of 15 μm sources in the HDF-N + FF, which is somewhat peaked at $z \sim 0.8$ (H. A. Aussel et al. 2001, in preparation) and indicates that 45% of galaxies with $0.1 < S_{15} < 0.4$ mJy are LIGs and 20% are ULIGs, with the remaining being normal and low-luminosity starburst galaxies (Elbaz et al. 2001).
4. The spectrum of the cosmic far-infrared background between 100 and 850 μm as measured by DIRBE and FIRAS on *COBE*.

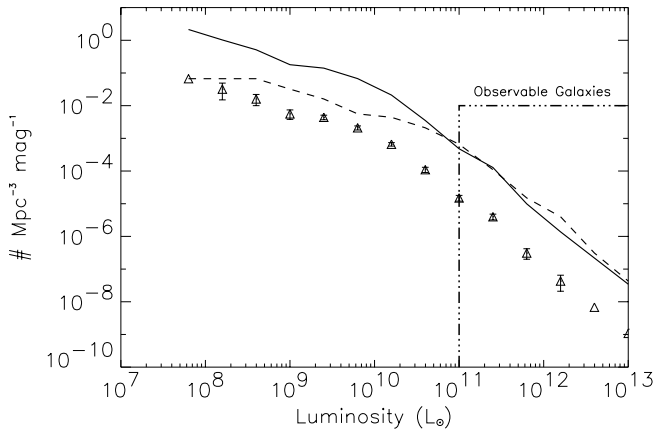

FIG. 6.—Degeneracy between luminosity and density evolution. The triangles are the extrapolated 60 μm LLF of Soifer et al. (1987), the solid line is the resultant luminosity function at $z \sim 1$ assuming a density evolution of $(1+z)^5$, while the dashed line is the luminosity function at $z \sim 1$ assuming a luminosity evolution of $(1+z)^2$. Also shown is the typical luminosity range of galaxies that have been detected by current long-wavelength surveys.

5. ISOPHOT 90 and 170 μm counts and SCUBA 850 μm number counts (Efstathiou et al. 2000; Hughes et al. 1998; Blain et al. 1999a; Barger et al. 1999; Eales et al. 2000; Dole et al. 2001).

The k-correction of galaxies illustrated in Figure 7 clearly illustrates the range of redshifts that can be studied by observations at these wavelengths. The 850 μm observations are typically confusion-limited at 2 mJy. However, deeper lensed surveys or using high-resolution radio interferometric data can push the detection threshold down to 0.5 mJy, which is past the confusion limit. This allows the detection of objects with $L_{\rm IR} > 5 \times 10^{11}\ L_\odot$ out to $z \sim 5$, which transforms to an SFR of greater than 85 $M_\odot\ {\rm yr}^{-1}$. On the other hand, the *ISO* mid- and far-infrared observations are typically dominated by galaxies at $z < 1$ and so can constrain the low-redshift turnover in the luminosity function evolution.

Figure 8 illustrates the nature of the counts if the 15 μm luminosity function remained equal to the local one at all redshifts, i.e., no evolution. The first plot shows the ISOCAM 15 μm differential counts from Elbaz et al. (1999), which include the *IRAS* 12 μm counts converted to 15 μm by Xu (2000) and the ELAIS 15 μm counts of Serjeant et al. (2000) renormalized as in Genzel & Cesarsky (2000). The remaining plots show the ISOPHOT FIRBACK 170 μm counts, ISOPHOT, *IRAS* BGS, and PSCz 90 μm counts, and SCUBA 850 μm integral counts. Also shown are the relative contributions from ULIGs, LIGs, and $L_{\rm IR} < 10^{11}$ $L_\odot$ galaxies to the counts at different wavelengths.[7] Clearly, some form of redshift evolution in the luminosity function is required to fit the counts. It should be emphasized that evolutionary models should be fitted to the differential counts at different wavelengths since integral counts tend to smooth over any subtle changes in the galaxy count slope. This requires that the calibration of the data from different surveys using the same instrument be consistent and accurate.

[7] From now on, we refer to the $L_{\rm IR} < 10^{11}\ L_\odot$ galaxies as normal/SB galaxies

The ISOPHOT 90 μm data are known to suffer from large calibration uncertainties that are not reflected in the error bars. We show in § 3.3 that our models fit the 170 μm counts but consistently overpredict the 90 μm counts, although both wavelengths probe similar populations of galaxies at $z < 1.2$. We find that an upward correction of the 90 μm flux densities by 30%, which is well within the calibration uncertainties, leads to excellent agreement between our models and the data. In addition, the faint-end PSCz counts are known to suffer from incompleteness (Efstathiou et al. 2000).

Any evolution of the luminosity function must have a turnover at some redshift $z_{\rm turn}$ to avoid overproducing the CIRB. In theory, the turnover redshifts $z^D_{\rm turn}$ ($z^L_{\rm turn}$), the α_D (α_L) value for the slope of the density (luminosity) evolution at $z < z_{\rm turn}$, and the β_D (β_L) value for $z > z_{\rm turn}$ can be different, implying that there are effectively six parameters. We, however, consider models with $z^D_{\rm turn} = z^L_{\rm turn}$ since it is unclear why the turnover for luminosity and density evolution, both of which are probably induced by galaxy interactions, should be different. The range of values for α, β, and $z_{\rm turn}$ selected for our models were $1 \le \alpha \le 6$, $-3 \le \beta \le 0$, and $0.6 \le z_{\rm turn} \le 1.5$, respectively. Evolutionary models with pure luminosity evolution and pure density evolution are also considered.

3.1. *Constraints on Pure Density Evolution*

We find that pure density evolution of the entire luminosity function cannot reproduce the counts at all the wavelengths. In this scenario, the 15 μm counts are dominated by the normal/SB galaxies, not by LIGs and ULIGs, which is inconsistent with observations in the HDF-N + FF. Second, the normal/SB galaxies are unable to reproduce the break in the 15 μm counts seen at 0.4 mJy but instead produce a sharp break only at $S_\nu < 0.2$ mJy.

However, density evolution models that evolve just a fraction of the 15 μm luminosity function, with the fraction being less than 5% at $L_{15\,\mu{\rm m}} \sim 10^9\ L_\odot$ and approaching 100% at 15 μm luminosities greater than $8 \times 10^{10}\ L_\odot$, provides reasonable fits to the data (dotted line in Fig. 14). The best-fit density evolution parameters then are $\alpha_D = 12.0 \pm 0.5$ up to $z^D_{\rm turn} = 0.7 \pm 0.1$ followed by $-0.5 < \beta_D \le 0$ (Fig. 9). The first plot shows the spectrum of the CIRB with lower limits from integrated counts of galaxies in the optical/UV from Madau & Pozzetti (2000), measurements in the near- and far-infrared using the DIRBE instrument (Hauser et al. 1998; Finkbeine, Davis, & Schlegel 1999; Gorjian et al. 2000; Wright 2001), an estimate of the far-infrared background from FIRAS (Lagache et al. 1999), and lower limits in the mid-infrared, far-infrared, and submillimeter from counts of individual galaxies (Elbaz et al. 1999; Blain et al. 1999a; Matsuhara et al. 2000). Also shown is the upper limit on the CIRB from TeV observations of Mrk 501 (Stanev & Franceschini 1998) and the cosmic microwave background at $\lambda > 300$ μm. The remaining plots show the counts for this evolution model.

Models with $\alpha_D > 13.0$ result in a significant overprediction of the 170 μm counts, while $\alpha_D < 11.0$ underpredicts the submillimeter counts. Changing the turnover redshift $z^D_{\rm turn}$ to high redshift shifts the knee in the 15 μm differential counts to fainter flux levels and vice versa. The slope of the evolution at $z^D_{\rm turn} > 0.7$ is mainly constrained by the spectrum of the CIRB at $\lambda > 200$ and the 850 μm counts.

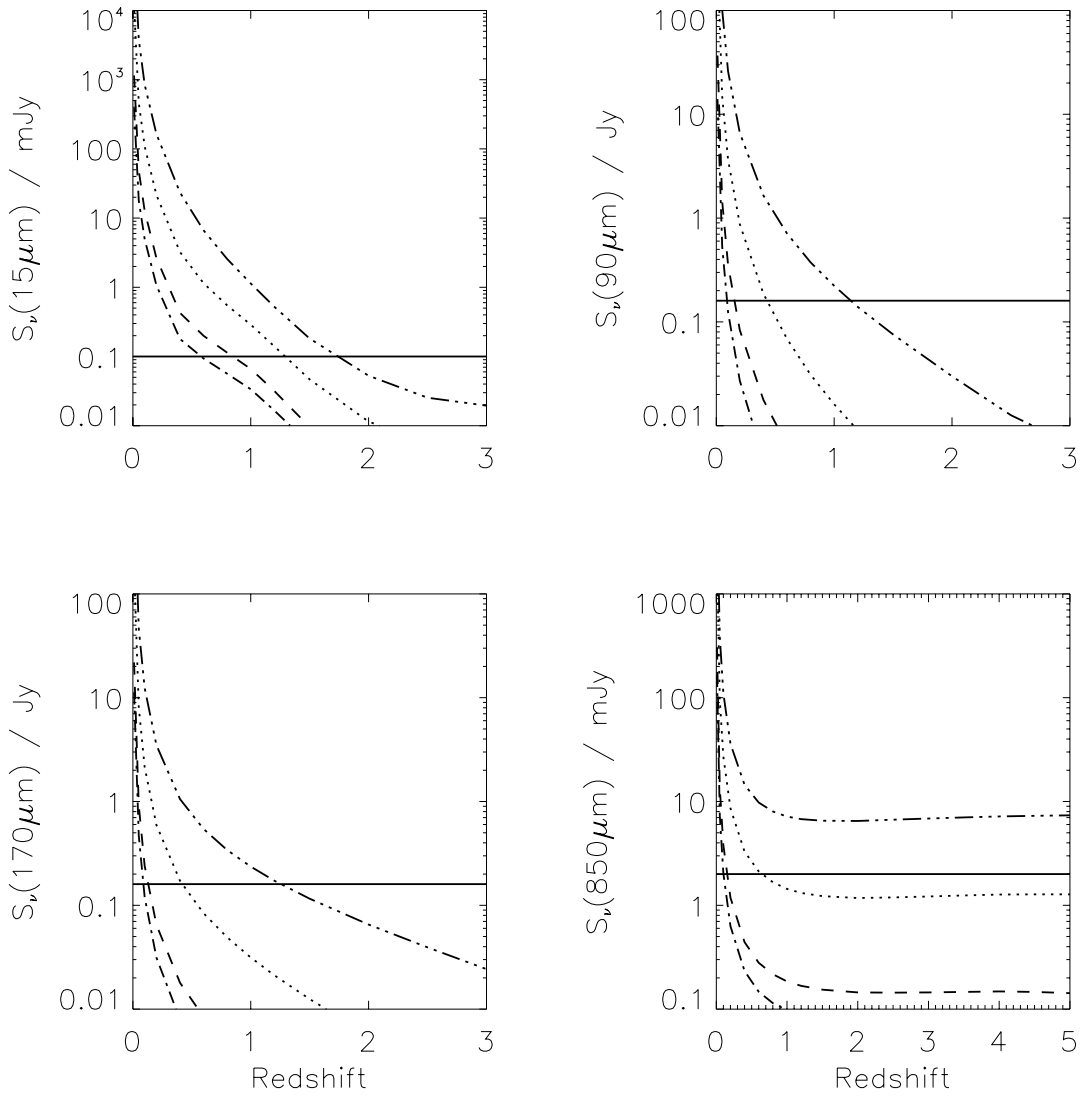

FIG. 7.—Predictions of flux densities at different wavelengths as a function of redshift for objects with an infrared luminosity of 10^{13} (*triple-dot–dashed line*), 10^{12} (*dotted line*), 10^{11} (*dashed line*) and 3×10^{10} $L_\odot$ (*dot-dashed line*). The solid horizontal line is the sensitivity of the deepest unlensed observation performed. The observations of lensing clusters at 15 μm are sensitive down to 50 μJy, while those at 850 μm are sensitive down to 0.5 mJy.

The 170, 90, and 15 μm observations all probe the population of galaxies at $z < 1.2$. However, in this density evolution model, the 15 μm counts are dominated ($\sim$90%) by LIGs and have an $\sim$5% contribution from ULIGs. In comparison, the 170 μm counts are dominated by ULIGs at redshifts between 0.5 and 1, while the 90 μm counts have roughly equal contributions from all three populations of galaxies. The 850 μm galaxies at flux densities larger than 1 mJy are mainly ULIGs at $z > 1$, while LIGs between redshifts of 0.6 and 2.0 dominate the counts at fainter flux levels.

The pure density evolution model shown appears to overpredict the contribution from LIGs ($\sim$90%) to the 15 μm number counts and underestimates the bright-end 850 μm counts. Second, many LIGs and ULIGs have been morphologically associated with disturbed systems. So a steep evolution in the density of objects should reflect in an increase of the merger fraction, which is defined as the fraction of galaxies in close pairs. Observationally, the merger fraction when averaged over all galaxies appears to evolve much slower with redshift, approximately as $(1 + z)^3$ (see, e.g., Le Fèvre et al. 2000). It is possible, though, that the LIGs and ULIGs have a merger fraction that increases much more rapidly than $(1 + z)^3$, but this has not been estimated since there are no clear observational signatures of LIGs and ULIGs at visible wavelengths. Although there is no strong observational evidence in favor of pure density evolution of a fraction of the luminosity function, we show in Figure 14 that it does predict the same number density of infrared luminous galaxies at high redshift as other models and so cannot be entirely ruled out.

3.2. *Constraints on Pure Luminosity Evolution*

We have shown above that some form of luminosity evolution is required to avoid deriving large values for the slope of the density evolution. The slope of the luminosity evolution α_L is strongly constrained by the mid-infrared number counts. Values of $\alpha_L < 4.5$ are unable to reproduce the break of the differential counts seen at a 15 μm flux density of 0.4 mJy, while $\alpha_L > 5.5$ results in an overproduction of

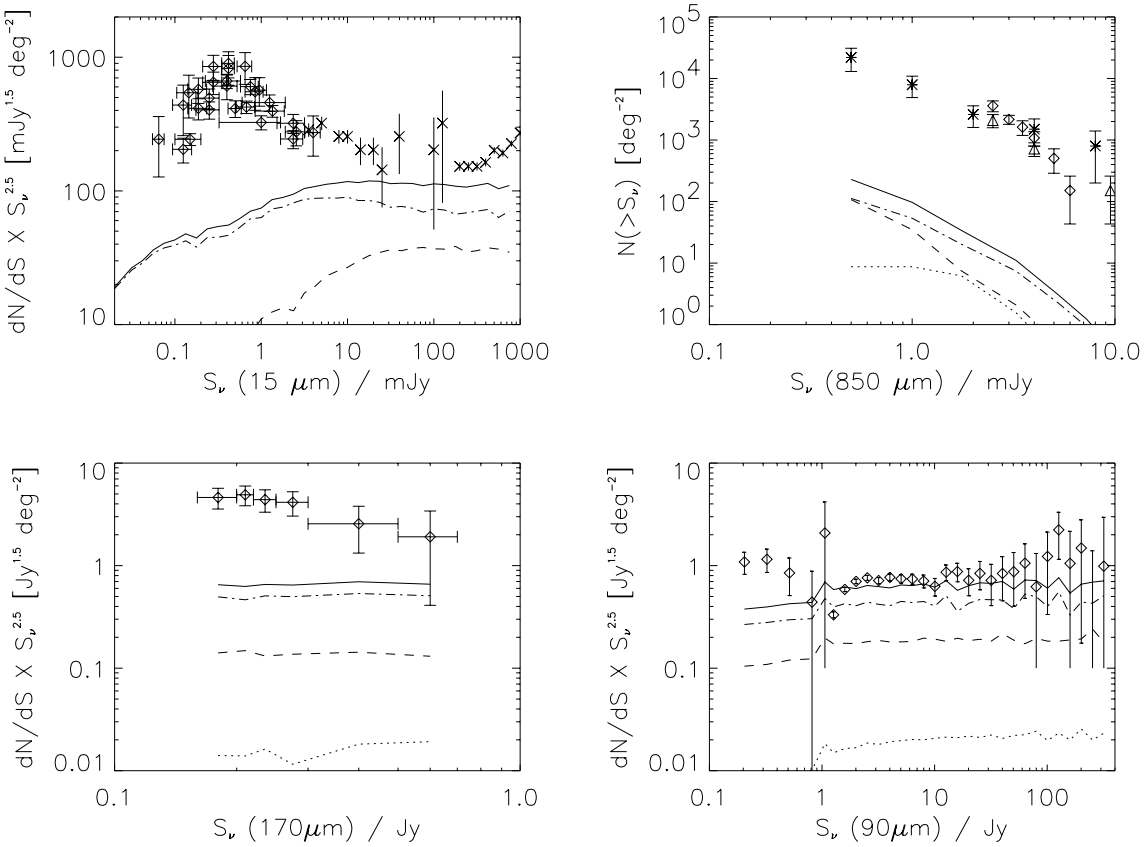

FIG. 8.—Results for a no-evolution model with thin solid line representing the contribution from all galaxies, with the dotted line indicating ULIGs only, the dashed line indicating LIGs only, while the dot-dashed line is for normal/starburst galaxies, i.e., $L_{\rm IR} < 10^{11}\ L_\odot$ (This convention will be used for the remaining figures as well). *Clockwise from top left*: (1) ISOCAM differential counts at 15 μm. Also shown are the bright-end *IRAS* counts of Xu (2000), which potentially have a factor of 2 uncertainty associated with them. (2) SCUBA 850 μm integral counts. (3) *IRAS* and ISOPHOT 90 μm differential counts. (4) ISOPHOT 170 μm differential counts (see text for references).

the counts at bright flux densities (Fig. 10). If the entire LLF is evolved (solid black line in Fig. 14), $\alpha_L = 5.0$ up to $z_{\rm turn}^L = 0.8$ followed by $-0.5 < \beta_L \leq 0.0$, the 90 μm differential counts are overproduced, but all the other counts are reproduced very well.

This is only partially consistent with the results of Xu (2000), who suggested that the mid-infrared counts can be modeled by evolving the entire LLF by $L(z) \propto (1+z)^{4.5}$ for $z < 1.5$ and by $L(z) = L(0) \times 2.5^{4.5}$ for higher redshifts. We find that a luminosity evolution of $(1+z)^{4.5}$ up to $z \sim 1$ followed by $L(z) = L(0) \times 2.0^{4.5}$ overpredicts the CIRB and provides only marginal fits to the mid-infrared counts at the faint end. Extending this evolution up to $z_{\rm turn}^L \sim 1.5$ severely overpredicts the CIRB as well as the observed faint-end 15 and 850 μm counts.

The main problem with pure luminosity evolution is that the 90 μm counts at $S_\nu < 6$ Jy are overproduced, but, as mentioned earlier, this can be resolved by rescaling the ISOPHOT 90 μm flux densities upward by 30%, which is within the calibration uncertainties of the instrument. In addition, the break in the 15 μm differential counts in this evolution model is not as sharp as observed.

As in the pure density evolution model, the counts at 15, 90, and 170 μm all trace galaxies at $z < 1.2$, but the relative contributions from LIGs, ULIGs, and normal/SB galaxies differ, with the 90 μm counts having roughly equal contributions from all three populations, the 170 μm counts being dominated by ULIGs, and the 15 μm counts being dominated by LIGs and low-redshift normal/SB galaxies. Pure luminosity evolution predicts that the contribution from normal/SB galaxies to the 15 μm counts between 0.1 and 0.4 mJy is 35%, similar to that observed in the HDF-N + FF. However, the contribution from ULIGs in the same flux density range is found to be only 6% in this model, which is a factor of 3–4 smaller than that observed.

3.3. *Combination of Luminosity and Density Evolution*

We have already illustrated the degeneracy and problems with pure luminosity and pure density evolution in the fits to the number counts. As illustrated above, both of them provide reasonable fits to the spectrum of the CIRB and to the differential counts at three wavelengths. An additional degeneracy is introduced when using a combination of luminosity and density evolution with only a fraction of the LLF evolving.

The fraction of the LLF that is evolving is defined as the "dusty starburst" population. We consider these to be galaxies with $L_B/L_{\rm IR} < 0.5$. This corresponds to $L_{\rm IR} \geq 10^{10.2}\ L_\odot$. All galaxies with $L_{\rm IR} \geq 10^{10.2}\ L_\odot$ are then evolved, while only about 5% of the galaxies with $L_{\rm IR} < 10^{10.2}\ L_\odot$ ("normal" galaxy population) are evolved, with a smooth transition between the two (dashed line in Fig. 14). We also considered models where the dusty starburst population is defined at a larger minimum luminosity ($L_{\rm IR} \sim 10^{11}\ L_\odot$) but

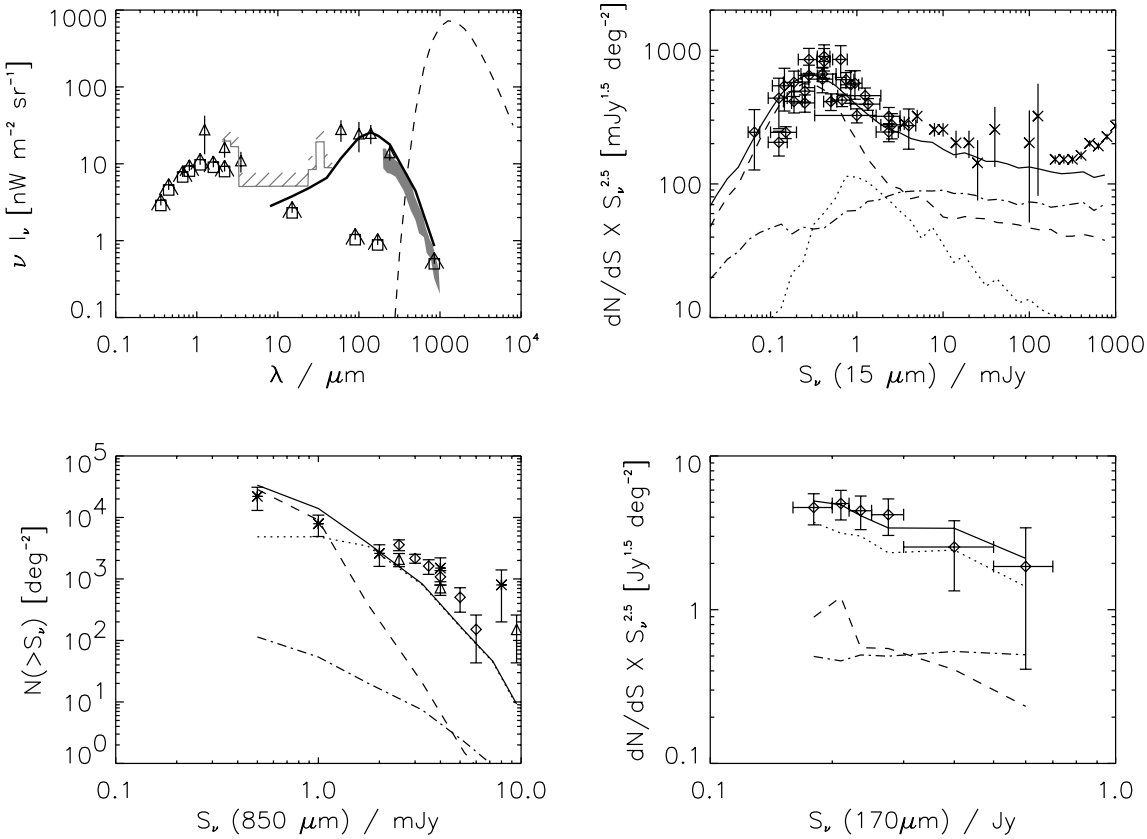

FIG. 9.—Results for the best-fitting pure density evolution model with only the most luminous end of the LLF evolving (dotted line in Fig. 14). The evolutionary parameters are $\alpha_D = 12.0$, $\beta_D = 0$, and $z_{\rm turn}^D = 0.7$. The upper left plot shows the spectrum of the CIRB: triangles represent the *COBE* DIRBE results, squares with upward arrows are lower limits from integrated counts at different wavelengths, the dark band is the FIRAS constraint, the hatched region represents upper limits from TeV gamma-ray observations of Mrk 501, the dashed line represents the cosmic microwave background, and the heavy solid line is the prediction from the model. The remaining plots are similar to Fig. 8.

were unable to find evolution parameters that could reasonably reproduce all the data.

Our best-fit model using a combination of both density and luminosity evolution for a fraction of the LLF as defined above is shown in Figure 11. Almost all the counts are reproduced quite well, with the exception of the 90 μm counts from ISOPHOT and PSCz, which all our models consistently overestimate. We interpret this to be due to a calibration error in the ISOPHOT data as a result of which the published flux density values are low by $\sim$30%. Also shown in the figure is the surface density of galaxies per redshift bin contributing to the counts at different wavelengths, as derived from the model, and the observed redshift distribution of the ISOCAM 15 μm galaxies in the HDF-N + FF (H. A. Aussel et al. 2001, in preparation). The size of each redshift bin is 0.2.

In the preceding three subsections, we have shown a range of models that evolve the local 15 μm luminosity function and fit the observed counts at mid- and far-infrared wavelengths as well as the spectrum of the CIRB. Ultradeep *SIRTF* observations at 24 μm can potentially break the degeneracy in these models if the counts can be determined to an accuracy of 20% or better (Fig. 12). The range of integral source counts that we predict based on our three evolutionary models (density, luminosity, and a combination of both) are 4.7, 3.8, and 3.7 arcmin^{-2} for $S_\nu > 120$ μJy and 19.8, 19.3, and 11.8 arcmin^{-2} for $S_\nu > 22$ μJy. However, the integral counts can be as low as 9.1 arcmin^{-2} at a flux density limit of 22 μJy for models that are at the extreme lower limit of the uncertainty in current observations.

4. THE ORIGIN OF THE CIRB

4.1. *Nature of the Galaxies Contributing to the CIRB*

In our evolution models, we have assumed that the contribution from active galactic nuclei (AGNs) to the counts and the cosmic background is insignificant. Other evolutionary models, which assumed an AGN component, arrived at the same conclusion (Malkan & Stecker 1998; Rowan-Robinson 2001; Xu et al. 2000; A. Franceschini et al. 2001, in preparation). Observational evidence for this assumption comes from deep *Chandra* observations of the HDF-N proper (Brandt et al. 2001), which detected eight of the ISOCAM 15 μm sources. However, only one of these is an AGNs at $z \sim 1$, and this was already known as such from observations at visible wavelengths (see discussion in Elbaz et al. 2001; H. A. Aussel et al. 2001, in preparation). It should be noted that it is insufficient to have an AGN in a galaxy to violate this assumption but that the integrated infrared light of the galaxy must be dominated by an AGN rather than by star formation. However, since the contribution of dust-enshrouded AGN at high redshift, beyond ISOCAM detection thresholds, is unknown, our results are

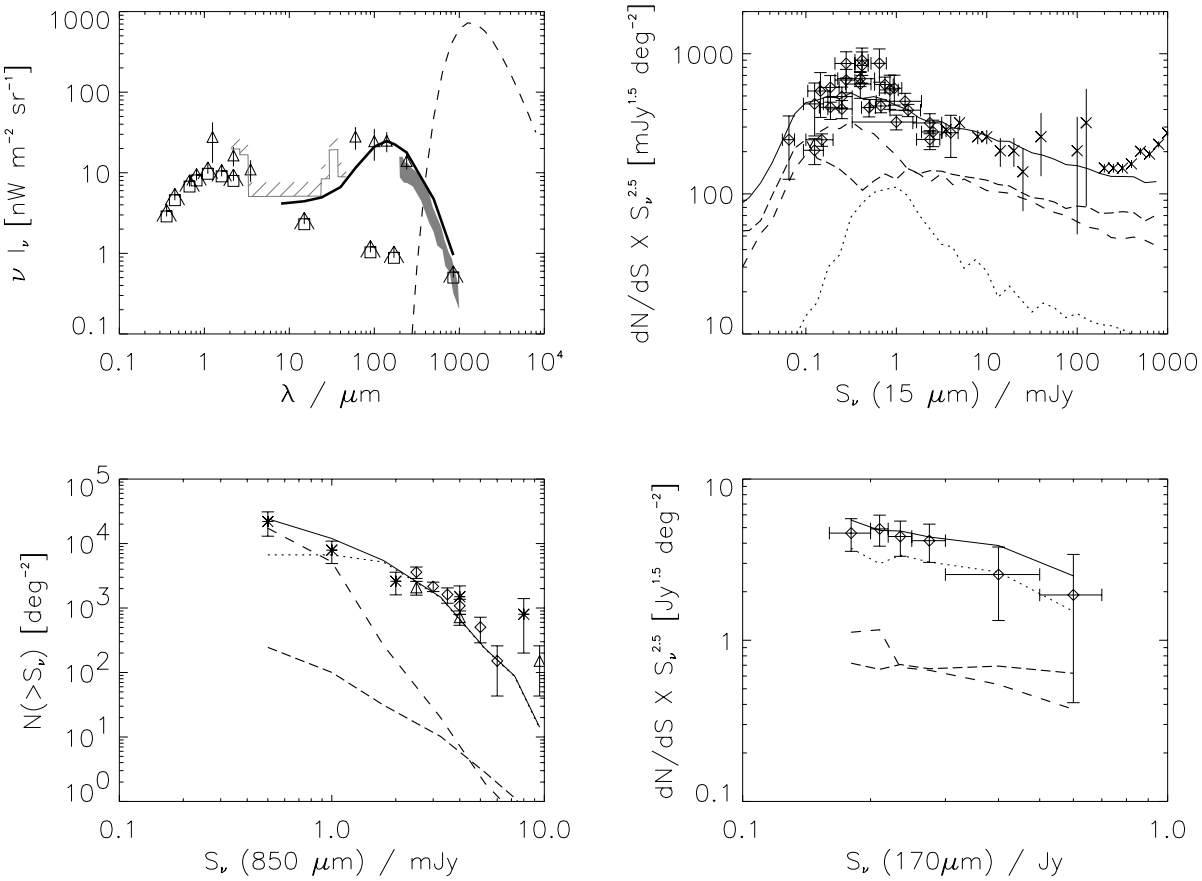

FIG. 10.—Results for the best-fitting pure luminosity evolution model of the entire LLF (solid black line in Fig. 14) with $\alpha_L = 5.0$, $\beta_L = 0$, and $z_{\rm turn}^L = 0.8$; $\beta_L = -0.25$ reduces the CIRB at $\lambda > 200$ μm but slightly lowers the bright-end SCUBA counts at flux densities greater than 2 mJy.

subject to this uncertainty. A large (>20%) contribution from AGNs to the source counts or the CIRB will imply a weaker redshift evolution of the luminosity function.

The evolution parameters in our model are constrained strongly by the ISOCAM counts at $z < 1.2$ and by the SCUBA counts at $z \sim 1$–3. In addition, the ISOCAM counts are dominated by LIGs, while the SCUBA counts are dominated by ULIGs. Thus, barring a dramatic change in the ratio of LIGs to ULIGs between a redshift of 1 and 2, we conclude that our models have robustly determined the evolution of the luminous end ($L_{\rm IR} > 10^{11}\ L_\odot$) of the LLF up to $z \sim 2$. At $z \gg 2$, the best constraint comes from the spectrum of the CIRB. Since all our models that are almost flat beyond $z \sim 2$ provide values for the CIRB that are at the upper limit of the values observed by FIRAS, we conclude that these models place a strong upper limit on the estimate of dust-enshrouded star formation at $z > 2$.

Our models indicate that about 80% of the 140 μm CIRB is produced at $z < 1.5$. In comparison, 90% of the 15 μm EBL, 65% of the 240 μm background, and only about 30% of the 850 μm background are produced within this redshift range (Table 1). We also derive that ISOCAM galaxies brighter than 0.1 mJy contribute 14.5 nW m^{-2} sr^{-1} to the 140 μm EBL, while galaxies brighter than 0.05 mJy produce 16.8 nW m^{-2} sr^{-1}. This accounts for about 75% of the total far-infrared background (Table 2). In comparison, we find that the contribution from SCUBA-detected galaxies brighter than the confusion limit of 2 mJy at 850 μm is only 3.4 nW m^{-2} sr^{-1} at 140 μm, while galaxies brighter than 0.5 mJy produce 16.4 nW m^{-2} sr^{-1}. This is because at 850 μm flux densities fainter than 1 mJy, the LIGs that dominate the ISOCAM counts and produce the majority of the 140 μm EBL contribute significantly to the SCUBA counts. The total EBL at 15 μm from our model is 3.2 nW m^{-2} sr^{-1}. The EBL obtained by integrating the observed ISOCAM counts above 50 μJy is 2.4 $\pm$ 0.5 nW m^{-2} sr^{-1} (Elbaz et al. 2001); hence, as much as 73% $\pm$ 15% of the 15 μm background might have already been resolved by ISOCAM. The models indicate that ULIGs contribute 15% of the 15 μm EBL observed by ISOCAM above 0.1 mJy, LIGs about 65%, and normal and low-luminosity starburst galaxies the balance. In comparison, at 140 μm, we find that ULIGs contribute 25% of the CIRB, LIGs contribute 60%, and normal/SB galaxies the balance (Fig. 13). Thus, infrared luminous galaxies, which appear to be indistinguishable from normal galaxies in terms of their optical/near-infrared luminosity and which form a negligible part of the energy budget in the local universe, dominate the star formation and therefore the energy budget at redshifts $z \sim 1$–3.

4.2. *Infrared Luminosity Function and the Lyman Break Galaxy Connection*

The first panel of Figure 14 shows the 15 μm LLF along with the fraction of galaxies that are evolved in the different models. For the density evolution model, the dotted line is evolved. For the luminosity evolution model, the whole 15 μm LLF, shown as the solid black line, is evolved. For the model with density + luminosity evolution, the dashed line is evolved. In the pure density evolution and density + luminosity evolution model, there is a non-

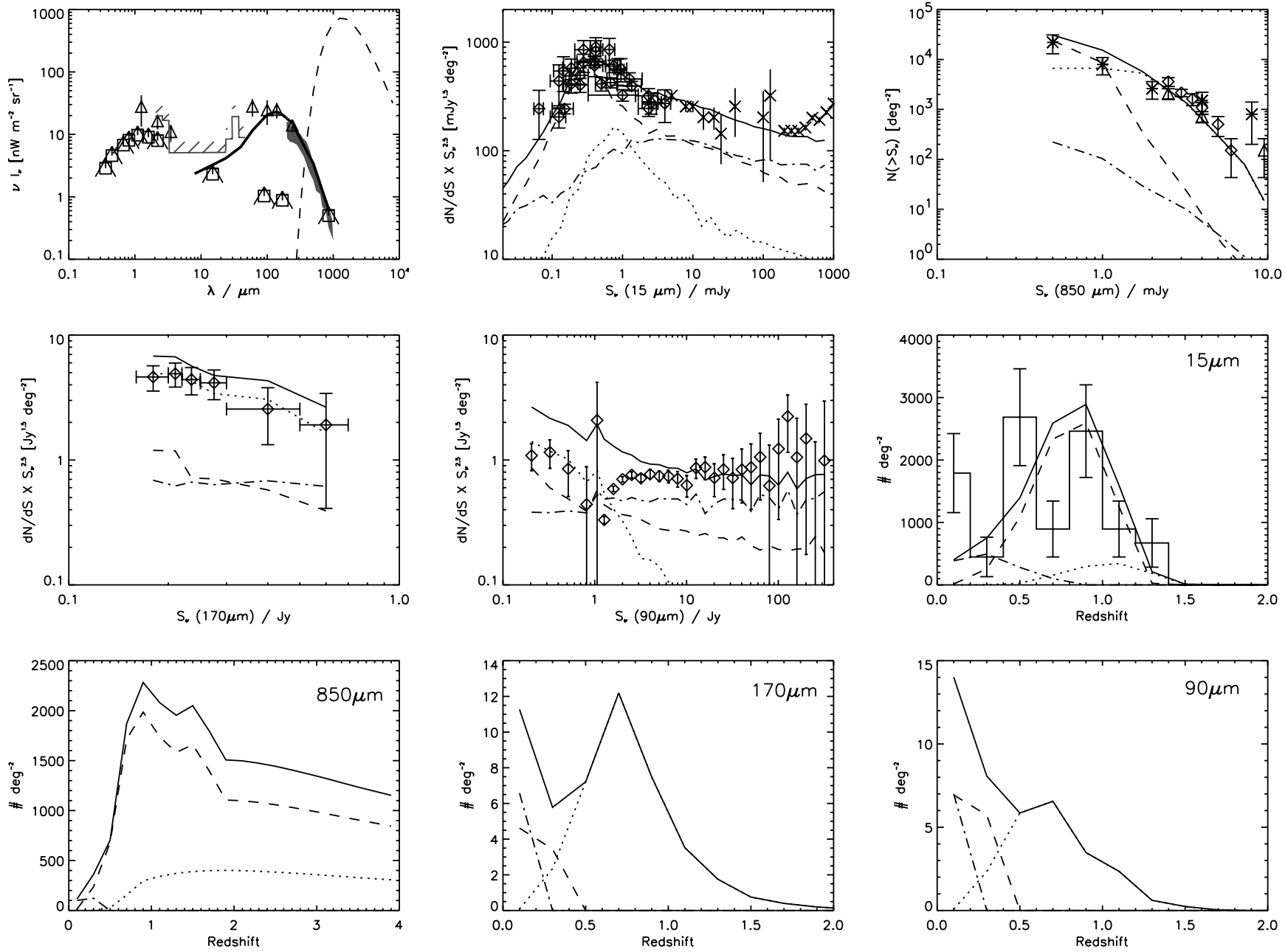

FIG. 11.—Results for a model with both luminosity and density evolution that evolves 5% of the luminosity function at $L_{\rm IR} < 10^{10.2}\ L_{\odot}$ and 100% at higher luminosities (dashed line in Fig. 14);$\alpha_L = 4.5$, $\alpha_D = 1.5$, $\beta_L = 0$, $\beta_D = -0.4$, and $z^L_{\rm turn} = z^D_{\rm turn} = 0.8$. The redshift distribution shown for galaxies with $S_\nu > 0.1$ mJy, 0.16 Jy, 0.16 Jy, and 0.5 mJy at 15, 90, 170, and 850 μm, respectively

TABLE 1

ORIGIN OF THE CIRB

WAVELENGTH (μm)	νI_ν (nW m^{-2} sr^{-1}) Observed	Model	CONTRIBUTION FROM $z < 1.5$ GALAXIES (%)
15	2.4 ± 0.5	3.2	90
24	...	4.2	83
140	25 ± 7	23.1	82
240	14 ± 3	15.1	67
850	0.5 ± 0.2	0.63	28

evolving component with a constant comoving density that corresponds to the difference between the total LLF and the evolving component.

Although the fraction of the luminosity function that is evolving and the evolutionary parameters are significantly different in our three evolutionary scenarios, we find that our models predict similar comoving number densities of infrared luminous galaxies at high redshift. This is illustrated in the two panels of Figure 14, which show the derived 15 μm luminosity function at redshifts of 0.4 and 0.8. The models also provide strong evidence for a change in the shape of the IRLF. The comoving number density of infrared luminous galaxies has to increase by more than 2 orders of magnitude between redshifts of 0 and 1 to fit the ISOCAM and SCUBA counts. The faint end of the LLF cannot be enhanced by the same factor since this would lead to an overproduction of the CIRB, although these galaxies would be below the sensitivity limit of the long-wavelength surveys. Lastly, as much as 85% of the far-infrared background can be attributed to infrared luminous galaxies. This implies that the contribution from normal and low-luminosity starburst galaxies ($L_{IR} < 10^{11}\ L_\odot$) to the dust-enshrouded SFR is relatively small. So, estimates of the total SFR made by applying a constant extinction correction to all optical/UV selected galaxies are incorrect. We conclude that long-wavelength surveys between 15 and 850 μm that probe galaxies at the luminous end of the IRLF provide a very effective way of tracing the bulk of the dust-enshrouded star formation.

The connection between infrared luminous galaxies and the Lyman break galaxy (LBG) population is intriguing. Figure 14 shows a comparison between the LBG 60 μm luminosity function at $z \sim 3$ of Adelberger & Steidel (2000, hereafter AS00), which was derived based on an extinction correction to optical/UV data as a function of the UV slope of individual galaxies, and our equivalent 60 μm luminosity function at $z \sim 3$, which we have argued earlier is only a strong upper limit. The agreement is extremely good considering that they were estimated in completely independent ways. The AS00 luminosity function predicts almost the same luminosity function as our estimate from the pure luminosity evolution model to within 50%. It is discrepant with the luminosity functions from our other two models by as much as an order of magnitude at the faint end but only by a factor of 2 at the bright end. As mentioned earlier, the long-wavelength surveys that constrain our models are mainly sensitive to the evolution of galaxies at the bright end of the luminosity function at $z < 2$. We are unable to constrain with much certainty the evolution of the faint end of the luminosity function, although we do place an upper limit based on the observed intensity of the CIRB. Further-

TABLE 2

ORIGIN OF THE 140 μM EBL AS DERIVED FROM THE MODELS

Source Type	Contribution (%)
ULIGs	25
LIGs	60
$L_{IR} < 10^{11} L_\odot$ galaxies	15
ISOCAM galaxies with $S_\nu(15\ \mu m) > 0.1$ mJy	63
ISOCAM galaxies with $S_\nu(15\ \mu m) > 0.05$ mJy	73
SCUBA galaxies with $S_\nu(850\ \mu m) > 2$ mJy	15
SCUBA galaxies with $S_\nu(850\ \mu m) > 0.5$ mJy	71

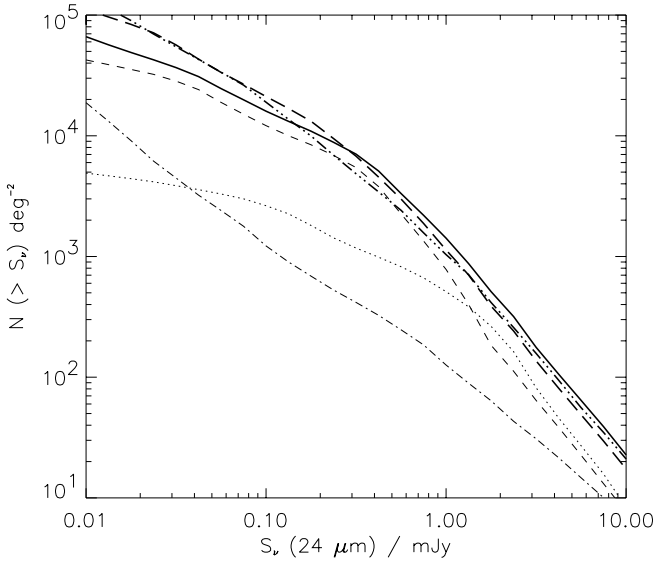

FIG. 12.—Prediction for integral source counts seen by *SIRTF* at 24 μm for the three different evolutionary models described in the text. The dashed line is for pure density evolution, the triple-dot–dashed line is for pure luminosity evolution, the solid line is for density + luminosity evolution, while the thin broken lines are contributions from ULIGs, LIGs, and $L_{IR} < 10^{11}\ L_\odot$ galaxies to the counts from the density + luminosity evolution using the convention defined in Fig. 8. [*See the electronic edition of the Journal for a color version of this figure.*]

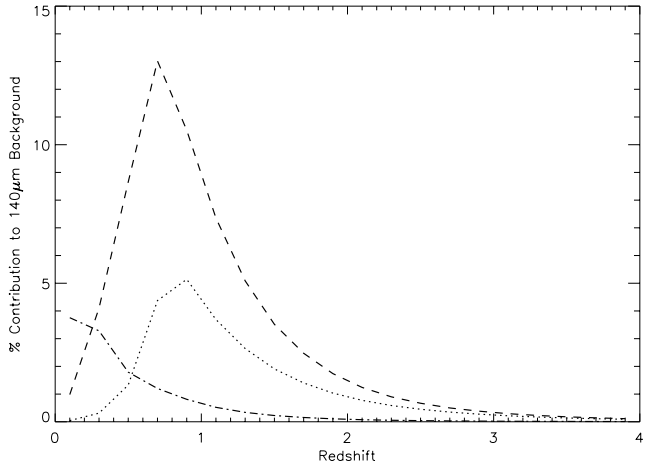

FIG. 13.—Plot showing the relative contribution of LIGs (*dashed line*), ULIGs (*dotted line*), and normal/starburst galaxies (*dot-dashed line*) to the 140 μm EBL as a function of redshift. Each redshift bin is 0.2.

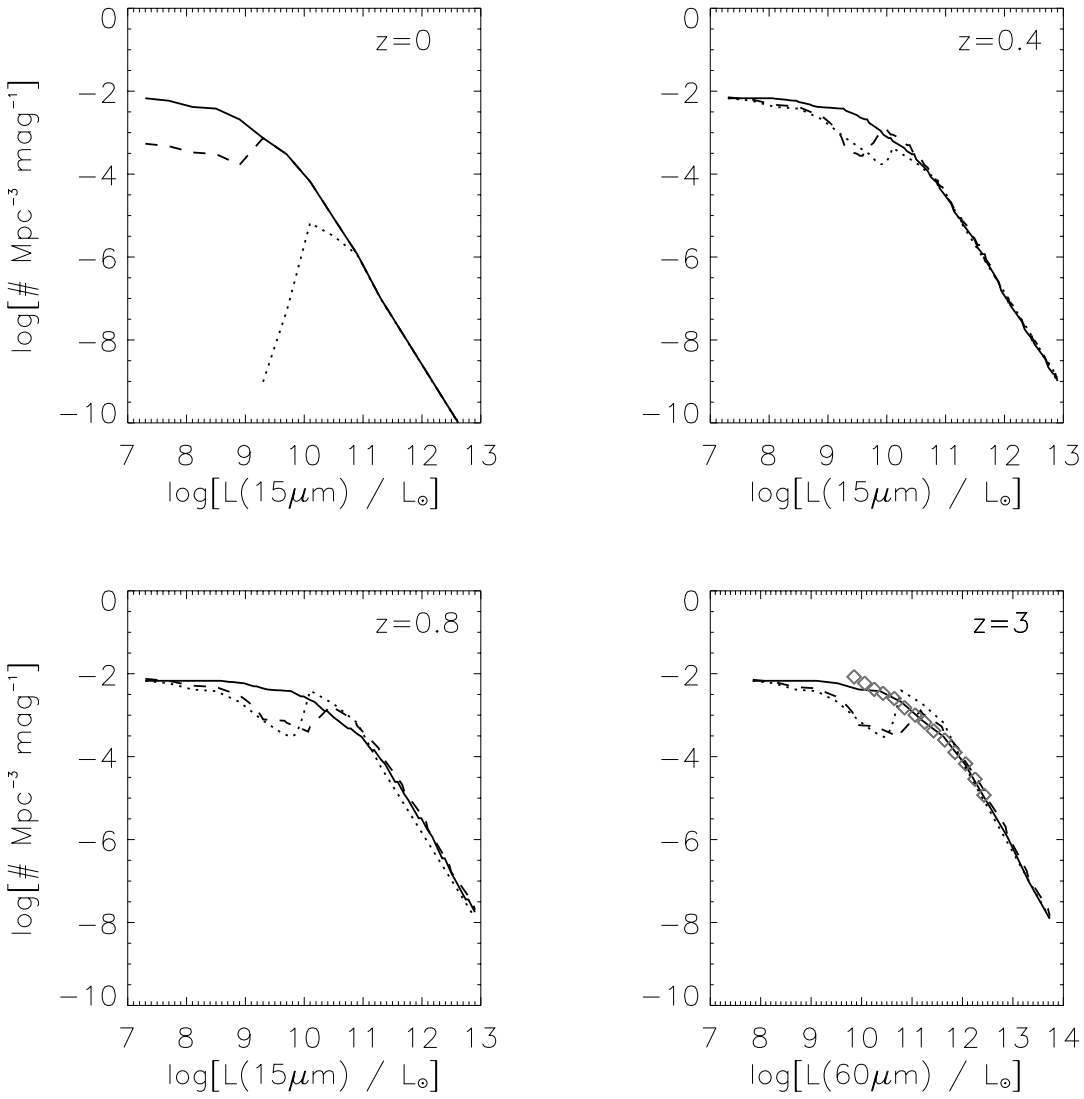

FIG. 14.—*Top left-hand panel*: Local 15 μm luminosity function (*solid line*). For pure luminosity evolution, we evolved the whole LLF; the dashed line is the starburst component that is evolved in the density + luminosity evolution model, and the dotted line is the luminous component that is evolved in pure density evolution models. *Top right-hand panel*: Total (evolving + nonevolving) 15 μm luminosity function for the three models at $z = 0.4$. *Bottom left-hand panel*: Total 15 μm luminosity function at $z = 0.8$. *Bottom right-hand panel*: 15 μm luminosity function at $z = 3$ converted to 60 μm and compared with the 60 μm LBG luminosity function (*diamonds*) of Adelberger & Steidel (2000). [*See the electronic edition of the Journal for a color version of this figure.*]

more, our estimates at $z \sim 3$ are only a strong upper limit to the number density of infrared luminous galaxies since any further evolution at high redshift overproduces the CIRB at $\lambda > 200$ μm, while a decay in the evolution at $z > 2$ as $[1 + (z - 2)]^{-2}$ is marginally consistent with both the submillimeter counts and the CIRB spectrum. Thus, we conclude that optical/UV surveys that trace the LBG population at $z > 3$, after an extinction correction factor that spans the 2–100 range, provide a good estimate of dust-enshrouded star formation at high redshift. They complement the results of future mid- and far-infrared surveys with *SIRTF*, which will be able to directly observe the dust emission of LBGs with LIG-type infrared luminosities up to $z \sim 2.5$.

There is observational evidence that the LBG population is distinct from the bright [$S_\nu(850\ \mu\text{m}) > 6$ mJy] submillimeter galaxies (Barger et al. 2000; Chapman et al. 2000). This is because most of the bright 850 μm galaxies are extreme ULIGs with $L_{\rm IR} > 10^{12.6}\ L_\odot$. The AS00 observations detect only two of 831 galaxies above this detection threshold, and only 27 of their LBG sample would have a submillimeter detection above the level of ~ 1 mJy. Second, at $z \sim 3$, the 850 μm observations would probe rest-frame ~ 200 μm emission. For a given far-infrared luminosity, the 60 μm luminosity shows a factor of 2–3 less scatter than the 850 μm luminosity among local galaxies (Fig. 3), suggesting that the $\lambda > 200$ μm spectral shape of galaxies might potentially have a larger scatter, which would lead to uncertain flux estimates on a galaxy-by-galaxy basis. Lastly, we do not find any scenario in which the contribution from ULIGs is greater than 30% of the comoving SFR at $z \sim 3$. Naturally, the contribution from extreme ULIGs traced by the bright submillimeter galaxies is even smaller. Thus, although the contribution to the SFR density from extreme ULIGs is missed in observations of the LBG population, their contribution is significant only at the level of less than 10%, and hence they are less important to an estimate of the high-redshift dust-enshrouded star formation.

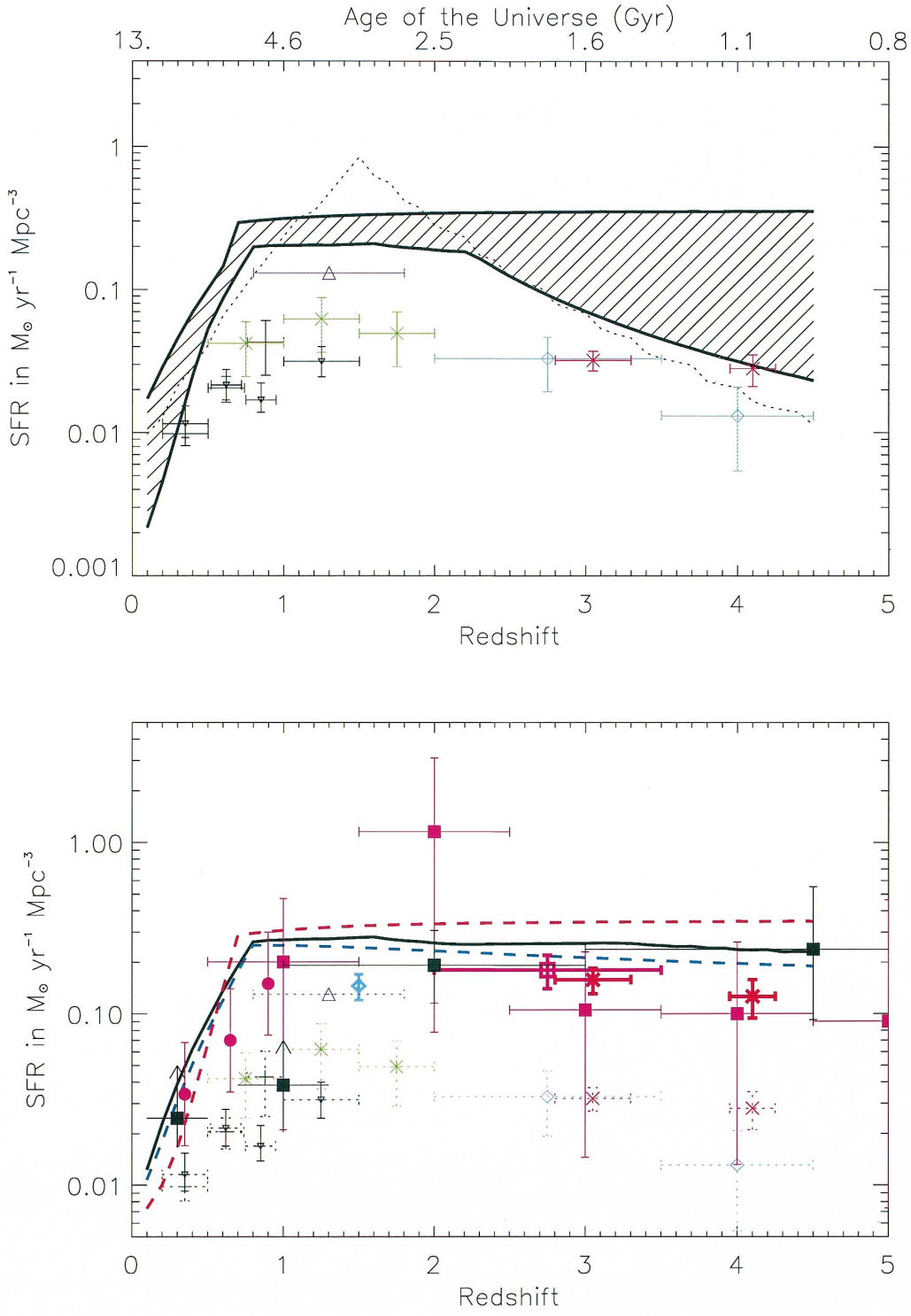

FIG. 15.—*Upper plot*: Absolute maximum and minimum range of values derived from our model for the obscured SFR density in comparison to observed optical/UV points in a $H_0 = 50$ km s^{-1} Mpc^{-1} and $q_0 = 0.5$ cosmology for comparison to other works. Data points are from Lilly et al. (1996). Madau et al. (1996), Connolly et al. (1997), Cowie et al. (1999), Steidel et al. (1999), and Yan et al. (1999); (*black plus signs, blue diamonds, green crosses, inverted triangles, red crosses, and purple triangles, respectively*). The dotted black line is the model of Xu et al. (2000). *Lower plot*: Our three models for the obscured SFR with the observed UV points as dotted symbols and the extinction-corrected estimates from Madau et al. (1998), Meurer et al. (1999), Steidel et al. (1999), and Thompson et al. (2001) as blue diamonds, open red squares, red crosses, and filled red squares, respectively. Also shown is the rate derived from *ISO* observations of the CFRS field (Flores et al. 1999) as filled red circles and estimates from the radio and submillimeter by Barger et al. (2000) as filled black squares. Our three evolutionary models are shown as a solid line (pure luminosity), a dashed red line (pure density), and a dashed blue line (density + luminosity). We assign a 1 σ error of 50% to our estimates of the dust-enshrouded SFR. We emphasize that our models only place a strong upper limit on the SFR at $z > 2$ and drop-off with redshift to agree with the extinction-corrected optical/UV measurements is consistent with both the submillimeter counts and the CIRB spectrum.

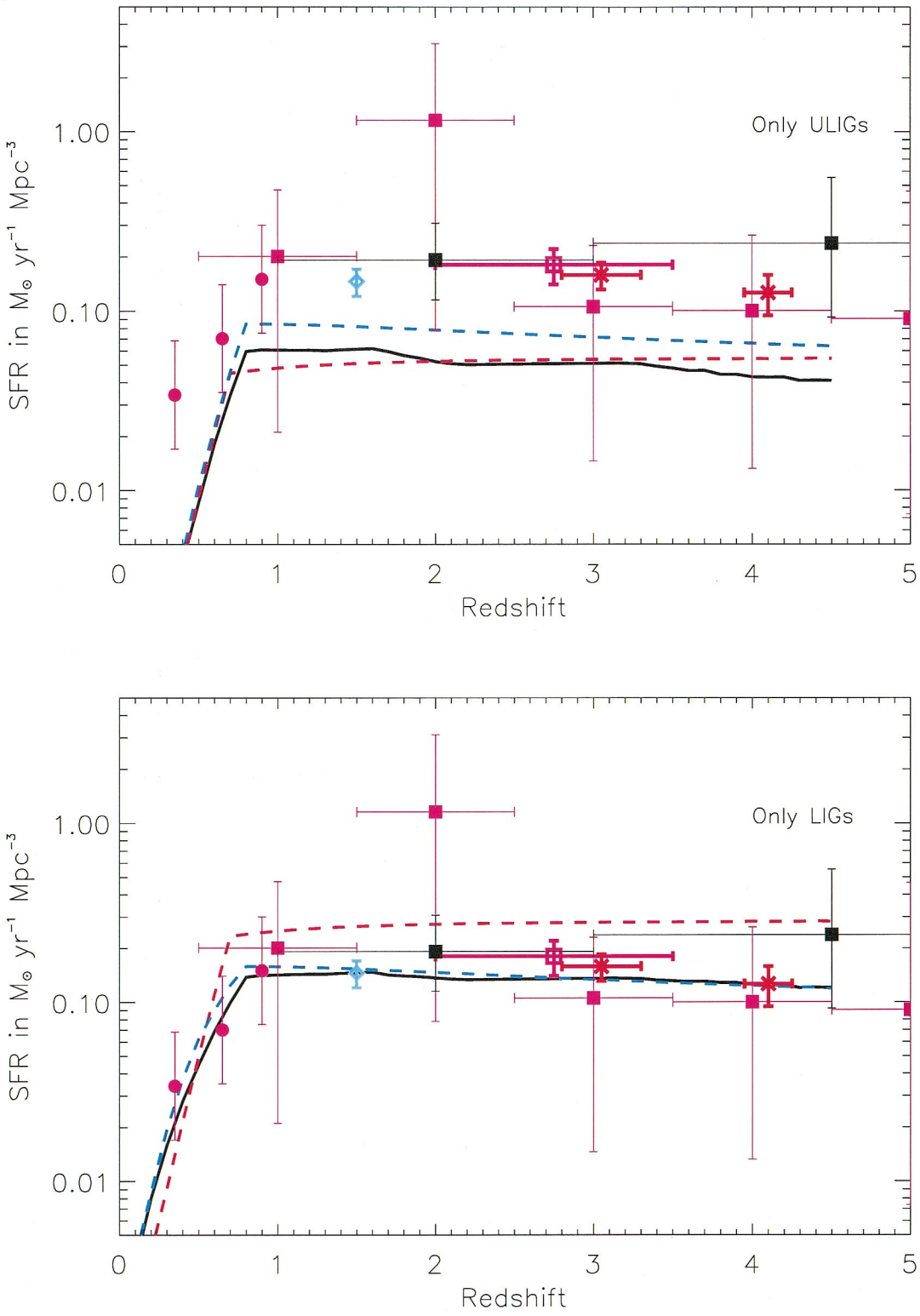

FIG. 16.—Plots showing the contribution to the dust-enshrouded SFR density from only LIGs and ULIGs as derived from our three models. A comparison with Fig. 15 shows that the contribution from normal/SB galaxies with $L_{IR} < 10^{11}\ L_\odot$ is relatively small at $z > 0.5$, ~5%–30% depending on the model. Symbols are the same as those in Fig. 15.

4.3. *The Revised Star Formation History of the Universe*

Having constrained the evolution of the mid-infrared and thereby the far-IRLFs, we can derive the evolution of the dust-enshrouded SFR with redshift. Using the equations listed in § 2, our derived comoving SFR from all galaxies is shown in Figure 15, while the separate contribution from LIGs and ULIGs is shown in Figure 16. Figure 15 also shows the absolute minimum and maximum range of dust-enshrouded SFR values. The maximum values are derived from models that marginally overproduce the CIRB and the counts. The minimum values are derived by using an evolutionary model that is marginally consistent with the

observations (§ 4.2) and by only considering the contribution from LIGs and ULIGs since those are the only galaxies that are directly observed at high redshift in the 15 and 850 μm surveys. Also shown are the SFR as inferred from direct observations at visible/UV/near-infrared wavelengths (Lilly et al. 1996; Madau et al. 1996; Connolly et al. 1997; Cowie et al. 1999; Steidel et al. 1999; Yan et al. 1999), SFR estimates obtained from extinction corrections to these observations (Madau et al. 1998; Meurer et al. 1999; Steidel et al. 1999; Thompson, Weymann, & Storrie-Lombardi 2001), and SFRs derived from ISOCAM observations of the Canada-France Redshift Survey field (Flores et al. 1999). In addition, lower limits to the SFR from radio measurements and two points representing the completeness corrected submillimeter observations are also shown (Barger et al. 2000). The 1 σ uncertainty in our derived rate is about 50% and is primarily dependent on the transformation from 15 μm to infrared luminosities, which, as derived earlier, has a 1 σ of 40%, and the transformation from infrared luminosities to SFR, which assumes a Salpeter initial mass function (IMF) and also has an uncertainty of about 30% (Kennicutt 1998).

The dust-enshrouded SFR density peaks at a redshift of 0.8 ± 0.1 with a value of $0.25^{+0.12}_{-0.1}\ M_\odot\ \mathrm{yr}^{-1}\ \mathrm{Mpc}^{-3}$. In a (0.3, 0.7, 75) cosmology, this corresponds to 6.2 Gyr after the Big Bang. The dusty SFR then remains almost constant up to $z \sim 2$, which corresponds to an age of 3 Gyr beyond which this value provides a strong upper limit to the amount of dust obscuration. This is similar to the shape of the star formation history preferred by Sadat et al. (2001) in their analysis of the CIRB. Our values are a factor of 2 larger than estimates at $z \sim 1$ from Hα observations by Yan et al. (1999) and a factor of 3–7 larger than extinction-uncorrected optical/UV observations at $z < 2$. The models are in excellent agreement with the submillimeter data corrected for incompleteness (Barger et al. 2000) but are higher than the Steidel et al. (1999) extinction-corrected points. The values we derive are systematically higher than those in Gispert, Lagache, & Puget (2000) but within the uncertainties, especially if the difference in the L_{IR}-to-SFR calibration coefficient is factored in. Our models also indicate a faster evolution at $z < 1$ than the models of Blain et al. (1999b), which is not surprising since they did not use the ISOCAM data to constrain their low-redshift evolution. However, our high-redshift plateau is similar to their Anvil-10 model.

Recently, Xu et al. (2000) have developed a multiparameter model in which the 25 μm luminosity function of Shupe et al. (1998) is partitioned into three components—starburst, late-type galaxies, and AGNs—and each component is evolved independently of the other. Specifically, they evolved the starburst population in luminosity as $(1 + z)^{4.2}$ and in density as $(1 + z)^2$ out to $z = 1.5$. The late-type galaxy population was evolved in luminosity as $(1 + z)^{1.5}$, while the galaxies with AGNs evolve in luminosity as $(1 + z)^{3.5}$. Beyond $z = 1.5$, all the components drop off as $(1 + z)^{-3}$. Using a 25 μm–to–IR luminosity conversion based on *IRAS* data, we have converted their evolution for starburst and late-type galaxies into an SFR and compared it with ours. This is shown as the black dotted line in the upper plot of Figure 15. We find that their derived rates between redshifts of 1 and 2.5 are inconsistent with our models. The motivation for this peak is not clear since only the CIRB and the SCUBA counts place constraints on the evolution at this redshift range and both can be reproduced very well by an almost flat evolutionary history at $z > 0.8$ (see § 3). However, their evolution at $z < 1$ agrees reasonably well with ours since both are principally constrained by the 15 μm ISOCAM counts. Furthermore, their decline in the SFR at high redshift ($z > 2$) is similar but below our lower limit.

By integrating our comoving SFR density over redshift and thereby cosmic time, we can derive the density of stars and stellar remnants and compare it with the total baryon density in the local universe. Stellar lifetimes were chosen for solar metallicity stars (Bressan et al. 1993), while the mass of remnants was chosen using the recipe of Prantzos & Silk (1999) and references therein. If a Salpeter IMF is assumed, then the model predicts a local density of baryons of about $1.0 \times 10^9\ M_\odot\ \mathrm{Mpc}^{-3}$, which is a factor of 2 in excess of the value of $(5 \pm 3) \times 10^8\ M_\odot\ \mathrm{Mpc}^{-3}$ estimated by Fukugita, Hogan, & Peebles (1998). The model also predicts that 100% of the local stars and remnants would have been produced at a redshift $z < 2.0$. If we instead use the shape of the IMF below 1 $M_\odot$ suggested by Gould, Bahcall, & Flynn (1996), which reduces the number density of low-mass stars, then the density of stars and remnants resulting from the model is $7.5 \times 10^8\ M_\odot\ \mathrm{Mpc}^{-3}$, which is in agreement with the local density. Madau & Pozzetti (2000) argued for a similar IMF based on their analysis of the total EBL. Interestingly, our model predicts that the local baryon density in stars and remnants, derived by integrating the star formation in ULIGs with a redshift distribution as shown in Figure 16, is similar to that seen in local spheroids, suggesting that high-redshift infrared luminous galaxies may be the progenitors of present-day spheroids.

5. CONCLUSIONS

A variety of observational data at mid-infrared through submillimeter wavelengths trace the fraction of emission from stars that is thermally reprocessed by dust. By using the counts of galaxies at these wavelengths, it is possible to estimate the amount of star formation that is enshrouded by optically thick H II regions and thereby invisible to observations at ultraviolet and visible wavelengths. In addition, the spectrum of the CIRB at mid- and far-infrared wavelengths places an upper limit on the fraction of starlight that has undergone thermal reprocessing by dust.

We have developed a set of template SEDs for galaxies as a function of infrared luminosity, which reproduce existing data at 0.44, 7, 12, 15, 25, 60, 100, and 850 μm from *ISO*, *IRAS*, and SCUBA on nearby galaxies. The 15 μm LLF was then evolved with redshift, taking both luminosity and density evolution models into account, and using the template SEDs to fit the observed counts at 15, 90, 170, and 850 μm. A number of evolutionary models provide reasonable fits to the data and the spectrum of the CIRB. The principal reason for this is that all the long-wavelength surveys are typically sensitive to only the most luminous galaxies ($L_{\mathrm{IR}} > 10^{11}\ L_\odot$) at $z > 0.5$. So, evolutionary models that result in similar luminosity functions at $L_{\mathrm{IR}} > 10^{11}\ L_\odot$ are degenerate. However, our models accurately constrain the comoving number density of these luminous galaxies as a function of redshift. In the local universe, it is these galaxies, many of which show morphological signatures of interaction, that show an infrared-determined SFR that is about an order of magnitude higher than the corresponding UV-determined SFR. By integrating the infrared luminosity of these luminous galaxies, we then obtain an estimate of the dust-enshrouded SFR. The dust-enshrouded SFR density

appears to peak at a much lower redshift than previously thought, at $z = 0.8 \pm 0.1$ with a value of $0.25^{+0.12}_{-0.1}\ M_\odot\ \mathrm{yr}^{-1}\ \mathrm{Mpc}^{-3}$, and remains approximately constant at least until $z \sim 2$. Any drop-off at a lower redshift would result in an underestimate of the 850 μm galaxy counts. Although our models do not constrain the evolution of the faint end ($L_{\mathrm{IR}} < 10^{10}\ L_\odot$) of the luminosity function, their net contribution to the high-redshift dust-enshrouded star formation is negligible, as can be seen in the range of evolutionary models considered. The evolution at $z > 2$ is constrained much more weakly. Having a constant SFR between redshifts of 0.8 and 4 is consistent with the CIRB spectrum and the submillimeter counts, as is a decay by a factor of 7 between redshift 2 and $\sim$5. However, we find that there is excellent agreement between our luminosity function and the IRLF derived from extinction correction to optical/UV observations of LBGs at $z \sim 3$. This suggests that dust obscuration is significant even at $z > 3$ and that the dust-enshrouded SFR is constant to within a factor of 2 between redshifts 2 and 4.

The models also provide a census of the luminosity of galaxies that contribute to the counts at different wavelengths, their redshift distribution, and the relative contribution to the CIRB at $\lambda > 5$ μm as a function of redshift. Furthermore, we find that ultradeep observations with *SIRTF* at 24 μm down to a sensitivity of 25 μJy can potentially break the degeneracy in the evolutionary models by detecting galaxies with $L_{\mathrm{IR}} \sim 10^{11.5}\ L_\odot$ out to $z \sim 2.5$, which is well beyond the turnover redshift of 0.8 that is derived from our models.

R. C. wishes to thank Harland Epps and Rodger Thompson for kindly funding this research through NASA grant NAG 5-3042. D. E. wishes to thank the American Astronomical Society for its support through the Chretien International Research Grant and Joel Primack, David Koo, and Joe Miller for supporting his research through NASA grants NAG 5-8218 and NAG 5-3507. We wish to acknowledge Pierre Chanial for collating published data from a large number of surveys and making them available to us.

REFERENCES

Adelberger, K., & Steidel, C. C. 2000, ApJ, 544, 218 (AS00)
Altieri, B., et al. 1999, A&A, 343, L65
Aussel, H. A., Coia, D., Mazzei, P., De Zotti, G., & Franceschini, A. 2000, A&AS, 141, 257
Barger, A. J., Cowie, L. L., & Richards, E. A. 2000, AJ, 119, 2092
Barger, A. J., Cowie, L. L., & Sanders, D. B. 1999, ApJ, 518, L5
Blain, A. W., Kneib, J.-P., Ivison, R. J., & Smail, I. 1999a, ApJ, 512, L87
Blain, A. W., Smail, I., Ivison, R. J., & Kneib, J.-P. 1999b, MNRAS, 302, 632
Brandt, W. N., et al. 2001, AJ, in press (astro-ph/0102411)
Bressan, A., Fagotto, F., Bertelli, G., & Chiosi, C. 1993, A&AS, 100, 647
Chapman, S. C., Richards, E. Lewis, G., Wilson, G., & Barger A. 2001, ApJ, 548, L147
Chapman, S. C., et al. 2000, MNRAS, 319, 318
Charmandaris, V., Laurent, O., Mirabell, I. F., Gallais, P. Sauvage, M., Vigroux, L., Cesarsky, C., & Tran, D. 1999, Ap&SS, 266, 99
Condon, J. J. 1992, ARA&A, 30, 575
Connolly, A. J., Szalay, A. S., Dickinson, M., Subbarao, M. U., & Brunner, R. J. 1997, ApJ, 486, L11
Cowie, L. L., Songaila, A., & Barger, A. 1999, AJ, 118, 603
Dale, D. A., Helou, G., Contursi, A., Silbermann, N. A., & Kolhatkar, S. 2001, ApJ, 549, 215
Désert, F.-X., Boulanger F., & Puget, J. L. 1990, A&A, 237, 215
Dole, H., et al. 2000, in *ISO* Surveys of a Dusty Universe, ed. D. Lemke, M. Stickel, & K. Wilke (Berlin: Springer)
———. 2001, A&A, 372, 364
Dunne, L., Eales, S., Edmunds, M., Ivison, R., Alexander, P., & Clements, D. L. 2000, MNRAS, 315, 115
Dwek, E., & Arendt, R. 1998, ApJ, 508, L9
Eales, S., Lilly, S., Webb, T., Dunne, L., Gear, W., Clements, D., & Yun, M. 2000, AJ, 120, 2244
Efstathiou, A., et al. 2000, MNRAS, 319, 1169
Elbaz, D., Cesarsky, C. J., Chanial, D., Aussel, H., Franceschini, A., Fadd, D., & Chary, R. 2001, A&A, submitted
Elbaz, D., et al. 1999, A&A, 351, L37
Fang, F., Shupe, D. L., Xu, C., & Hacking, P. B. 1998, ApJ, 500, 693
Finkbeiner, D. P., Davis, M., & Schlegel, D. J. 1999, ApJ, 524, 867
Fixsen, D. J., Dwek, E., Mather, J. C., Bennett, C. L., & Shafer, R. A. 1998, ApJ, 508, 123
Flores, H., et al. 1999, ApJ, 517, 148
Forster-Schreiber, N. M., Genzel, R., Lutz, D., Kunze, D., & Sternberg, A. 2001, ApJ, in press (astro-ph/0101153)
Franceschini, A., et al. 2001, A&A, submitted
Fukugita, M., Hogan, C. J., & Peebles, P. J. E. 1998, ApJ, 503, 518
Genzel, R., & Cesarsky, C. 2000, ARA&A, 38, 761
Gispert, R., Lagache, G., & Puget, J.-L. 2000, A&A, 360, 1
Gorjian, V., Wright, E. L., & Chary, R. R. 2000, ApJ, 536, 550
Gould, A., Bahcall, J. N., & Flynn, C. 1996, ApJ, 465, 759
Hauser, M., et al. 1998, ApJ, 508, 25
Hughes, D. H., et al. 1998, Nature, 394, 241
Kennicutt, R. C., Jr. 1998, ARA&A, 36, 189
Kim, D.-C., & Sanders, D. B. 1998, ApJS, 119, 41
Lagache, G., Abergel, A., Boulanger, F., Désert, F. X., & Puget, J.-L. 1999, A&A, 344, 322
Laurent, O., Mirabel, I. F., Charmandaris, V., Gallais, P., Madden, S. C., Sauvage, M., Vigroux, L., & Cesarsky, C. 2000, A&A, 359, 887
Le Fèvre, O., et al. 2000, MNRAS, 311, 565
Lilly, S. J., Le Fèvre, O., Hammer, F., & Crampton, D. 1996, ApJ, 460, L1
Madau, P., Ferguson, H. C., Dickinson, M. E., Giavalisco, M., Steidel, C. C., & Fruchter, A. 1996, MNRAS, 283, 1388
Madau, P., & Pozzetti, L. 2000, MNRAS, 312, L9
Madau, P., Pozzetti, L., & Dickinson, M. 1998, ApJ, 498, 106
Malkan, M. A., & Stecker, F. W. 1998, ApJ, 496, 13
———. 2001, ApJ, in press (astro-ph/0009500)
Mann, R. G., et al. 1997, MNRAS, 289, 482
Mathis, J. S. 1990, ARA&A, 28, 37
Matsuhara, H., et al. 2000, A&A, 361, 407
Meurer, G. R., Heckman, T. M., & Calzetti, D. 1999, ApJ, 521, 64
Meurer, G. R., Heckman, T. M., Seibert, M., Goldader, J. D., Calzetti, D., Sanders, D., & Steidel, C. C. 2001, in Cold Gas and Dust at High Redshift, ed. D. J. Willner (Highlights of Astronomy, Vol. 12; Dordrecht: Kluwer), in press (astro-ph/0011201)
Mirabel, I. F., et al. 1998, A&A, 333, L1
Pearson, C. 2001, MNRAS, in press (astro-ph/0011335)
Prantzos, N., & Silk, J. 1998, ApJ, 507, 229
Puget, J.-L., Abergel, A., Bernard, J.-P., Boulanger, F., Burton, W. B., Désert, F. X., & Hartmann, D. 1996, A&A, 308, L5
Puget, J.-L., & Leger, A. 1989, ARA&A, 27, 161
Richards, E. A., Kellermann, K. I., Fomalont, E. B., Windhorst, R. A., & Partridge, R. B. 1998, AJ, 116, 1039
Rigopoulou, D., Spoon, H. W. W., Genzel, R., Lutz, D., Moorwood, A. F. M., & Tran, Q. D. 1999, AJ, 118, 2625
Roussel, H., et al. 2001, A&A, 369, 473
Rowan-Robinson, M. 2001, ApJ, 549, 745
Rush, B., Malkan, M. A., & Spinoglio, L. 1993, ApJS, 89, 1
Sadat, R., Guiderdoni, B., & Silk, J. 2001, A&A, 369, 26
Sanders, D. B., & Mirabel, I. F. 1996, ARA&A, 34, 749
Saunders, W., Rowan-Robinon, M., Lawrence, A., Efstathiou, G., Kaiser, N., Ellis, R. S., & Frenk, C. S. 1990, MNRAS, 242, 318
Saunders, W., et al. 2000, MNRAS, 317, 55
Schlegel, D., Finkbeiner, D., & Davis, M. 1998, ApJ, 500, 525
Serjeant, S., et al. 2000, MNRAS, 316, 768
Shupe, D., Fang, F., Hacking, P. B., & Huchra, J. P. 1998, ApJ, 501, 597
Silva, L., Granato, G. L., Bressan, A., & Danese, L. 1998, ApJ, 509, 103
Smith, C. H., Aitken, D. K., & Roche, P. F. 1989, MNRAS, 241, 425
Soifer, B. T., Sanders, D. P., Madore, B. F., Neugebauer, G., Danielson, G. E., Elias, J. H., Lonsdale, C. J., & Rice, W. L. 1987, ApJ, 320, 238
Soifer, B. T., Sanders, D. P., Neugebauer, G., Danielson, G. E., Lonsdale, C. J., Madore, B. F., & Persson, S. E. 1986, ApJ, 303, L41
Stanev, T., & Franceschini, A. 1998, ApJ, 494, L159
Steidel, C. C., Adelberger, K. L., Giavalisco, M., Dickson, M., & Pettini, M. 1999, ApJ, 519, 1
Thompson, R., Weymann, R. J., & Storrie-Lombardi, L. 2001, ApJ, 546, 694
Tran, Q. D., et al. 2001, ApJ, 552, 527
Wright, E. L. 2001, ApJ, 553, 538
Wright, E. L., & Reese, E. D. 2000, ApJ, 545, 43
Xu, C. 2000, ApJ, 541, 134
Xu, C., et al. 1998, ApJ, 508, 576
Xu, C., Lonsdale, C. J., Shupe, D. L., O'Linger, J. & Masci, F. 2000, ApJ, submitted (astro-ph/0009220)
Yan, L., McCarthy, P. J., Freudling, W., Teplitz, H. I., Malumuth, E. M., Weymann, R. J., & Malkan, M. A. 1999, ApJ, 519, L47